New Insights and Trends in Transition Metal Ion Electron Paramagnetic Resonance[1]

John R. Pilbrow

Physics Department
Monash University
Clayton Victoria
Australia, 3168

Contents

I. Introduction 33

II. Review of Some Basic EPR Theory 34

III. New Insights into EPR (S=1/2) 36

IV. Implications of Field-Sweep 36
A. Complications for S=3/2 (4) 36
B. Linewidth Anisotropy 39
C. Introduction to Frequency-dependent or *g*-strain broadening 40

V. Low Frequency EPR 41

VI. Computer Simulations – Inclusion of Strain Broadening 43
A. Intercalation of Planar copper(II) complexes in DNA (26) 48
B. Generalized *g*-strain Broadening 49
C. Use of the Joint Density Function 50
D. Strategies for Powder/Frozen solution analysis 51
E. Powder Simulations $S > 1/2$. 51

VII. Orientation and Angular Modulation – Site Selectivity 52

VIII. Effective *g*-Factors for S=3/2 55

IX. Non Kramers Ions and Non Kramers Doublets (97) 56

X. Spin Lattice Relaxation 59

XI. Conclusion 60

[1]Based upon a Plenary Lecture presented to the 10th International Symposium on Electron Paramagnetic Resonance, Denver, Colorado, August 3, 1987

I. Introduction

It is a formidable task to present even a personal account of what seem to be the major events in the interpretation of the EPR of transition metal ions over the last decade or so, and it cannot do justice to everything that has happened. By the early 1970's the generally accepted view of EPR was that the spin-Hamiltonian and the various crystal and ligand field theories then current were adequate to cover most circumstances. There was a growing awareness that low symmetry systems represented a poorly understood area. Some new trends can be discerned since that time which represent a shift in the center of gravity of EPR theory and practice away from the determination of the spin-Hamiltonian for transition metal ions in a variety of crystalline environments, chemical complexes and biomolecules to a deep underlying concern about the origin of lineshapes and dynamical behavior. Since about 1974, in areas as diverse as the EPR of transition metal ions in glasses and proteins, considerable new insights into the origin of random strain effects and their effect on EPR spectra have been considered. Increasingly, new twists to old problems are being found and fascinating new challenges have emerged even in well-worked areas such as metallo-porphyrins and related compounds. A much improved understanding of the fundamental basis of field-swept EPR has emerged more recently and with that some very worthwhile consequences resulting from the non-equivalence of field- and frequency sweeps.

Electron Paramagnetic Resonance of Transition Ions by Abragam and Bleaney (1) was published in 1970. While it showed that EPR had come of age, it left untouched a number of fundamental issues especially concerning the nature of magnetic field-swept spectroscopy.

In some ways, 1975 was a watershed year, marked by the publication of the well-known paper by Aasa and Vanngard (2), in which they introduced the 1/g factor for spin 1/2, and a particularly insightful paper by Coffman (3). Both of these, in different contexts, dealt with aspects of the connection between field- and frequency-swept EPR. Further developments were needed and the author and his colleagues showed, first of all, that asymmetric lines should be expected in field-swept EPR (4). Subsequently a number of very interesting consequences of the correct way to think about an EPR transition have been identified (5). These include some new insights into linewidth anisotropy, the true origin of the $1/g$ factor, but also the fact that it is not necessary to use it, and strain broadening (5, 6). It now emerges that, along with eigenvectors and transition intensities, it is energy differences, and not resonance fields, that are the most important quantities to calculate. A transition remains a transition irrespective of whether frequency-sweep or field-sweep is used, for the same master equation handles both. While it has led, however, to an approximate doubling of computer simulation time, it is a price worth paying in order to be able to work within the simplest conceptual framework. It is becoming increasingly clear in cases of strain broadening, that the linewidth parameter, in frequency units, actually changes over the line. One can of course argue that if strain effects provide the only sources of line broadening, they enter through a random distribution in one or more parameters of the system, but where individual transitions are assumed to have their natural linewidths. It is appropriate to think in terms of an ensemble of paramagnetic ions in statistically distributed environments.

It used to be thought that for increased resolution of $S= 1/2$ spectra, experiments should be carried out at frequencies higher than the usual X-band. Therefore experiments were commonly carried out at Q-band. The insight provided by Hyde and his colleagues in Milwaukee late in 1978 changed all that (7). The variation in widths of parallel copper lines in frozen solution and powder spectra, the well-known m_I effect, turned out to have a frequency, or field-dependence as well (8). Optimum resolution for frozen solutions occurs in the S-band. Subsequently the advent of loop-gap resonators has provided many laboratories with quite satisfactory sensitivity at these lower frequencies. There are many compelling reasons for such experiments in addition to earlier motivations for reasons of reduced dielectric loss in aqueous solutions. This has put pressure on new developments in computer simulation of powder spectra and, in particular, it has led to the need for better models to describe strain broadening.

Twenty years ago a lecture with this title would have focused on the numerical or perturbation theory methods of solution needed to arrive at the best set of spin Hamiltonian parameters. Indeed, during that period, many journals implied that the spin

Hamiltonian is equivalent to the spectrum! While determination of spin Hamiltonian parameters remains a necessary goal in EPR, it is true to say that the ground has shifted. Refinement of spin Hamiltonian parameters more often than not nowadays involves use of confirmatory computer simulations which are then compared with experiment, paying as much attention to details of line profiles as theoretical insights allow.

Another trend can be discerned. The inadequacies of purely static models of the ligand field are now more widely recognized and, wherever possible, dynamical effects are included explicitly. In particular, the resurgence of interest in the Jahn-Teller effect, reflected in the recent books by Bersuker (9a) and the volume edited by Wagner and Perlin (9b), highlight the importance of vibronic interactions in EPR.

This review will be concerned almost exclusively with CW-EPR of paramagnetic systems where magnetic dilution ensures that the centers are relatively well isolated from one another. Such dilution is well ensured in proteins. Passing reference will be made to ENDOR, electron spin echo envelope modulation (ESEEM) and ENDOR-INDUCED EPR (EI-EPR). A consistent understanding of field-swept EPR is described which leads to an explanation of asymmetric lineshapes, highly anisotropic linewidths in very anisotropic spin 1/2 systems and frequency-dependent hyperfine linewidths. Interesting examples of line narrowing at S-band are also given. A consistent statement of more sophisticated strain broadening mechanisms are also given within the same framework. This paper will be a review of the past decade or so highlighting the role now played by statistical models of line broadening, of increased understanding of the complex anisotropy of linewidths even for axial systems. Recent work in the author's laboratory on non-Kramers ions will also be mentioned.

II. Review of Some Basic EPR Theory

Electron paramagnetic resonance (EPR), sometimes called electron spin resonance (ESR), is the resonant absorption of microwave radiation by a paramagnetic system. The spectra are due to magnetic dipole transitions measured at a constant microwave frequency (usually $\nu \sim 9$ GHz) by varying the applied magnetic field. This is in contrast to other single phonon spectroscopic techniques in which wavelength, or frequency, is varied. At a microwave frequency ~9 GHz, the potential resolution for transition ion spectra is ~ 0.0001 cm^{-1}. Paramagnets in this context are magnetically 'dilute' systems consisting of relatively well-isolated magnetic moments due to transition metal ions in crystals, metal complexes, organic radicals, biomolecules and other materials such as glasses.

Transition ions in crystalline or molecular environments are subject to a crystal or ligand field due to interactions between themselves and the surrounding atoms or ions. Such crystal or ligand fields perturb the well-known free-ion energy levels in characteristic ways according to the symmetry and position of the neighboring atoms. For odd electron or Kramers ions, the lowest energy states are always Kramers doublets and resonance is obtained between the Kramers levels split by the magnetic field.

Without going into any detail, it is worth pointing out that crystal field theories (CFT's) (10) are what Gerloch (12) calls 'global' models for they do do not immediately take into account in an intuitively self-evident way the effect of changing a particular ligand or a lowering of the symmetry. The superposition model (SPM) (11) and angular overlap model (AOM) (12) are 'local' models in the sense that the parameters associated with an individual coordinating ligand atom are included explicitly. For d-electron systems, the calculations in all of these models are carried out within in a d-orbital basis.

It used to be considered that the most important equation in EPR was the spin Hamiltonian. Nowadays it is seen more clearly as one of three rather important kinds of equations needed to understand transition ion EPR. The spin Hamiltonian is an effective Hamiltonian (1, 13, 14) that describes the isolated, low-lying electronic levels of a paramagnetic ion in terms of an effective electron spin S:

$$H = \beta \mathbf{S} \cdot \mathbf{g} \cdot \mathbf{B} + \mathbf{S} \cdot \mathbf{A} \cdot \mathbf{I} + \mathbf{I} \cdot \mathbf{P} \cdot \mathbf{I} + H_{fs} + \sum_{i=1}^{n} H^{i}_{ligand} \quad (1)$$

where β is the Bohr magneton, S the effective electron spin, $\mathbf{B}$ the magnetic field, I the nuclear spin, $\mathbf{g}$ the g-matrix, $\mathbf{A}$ the hyperfine matrix and P the electric quadrupole tensor. H_{fs} represents the so-called fine structure which is expressed as the sum of sym-

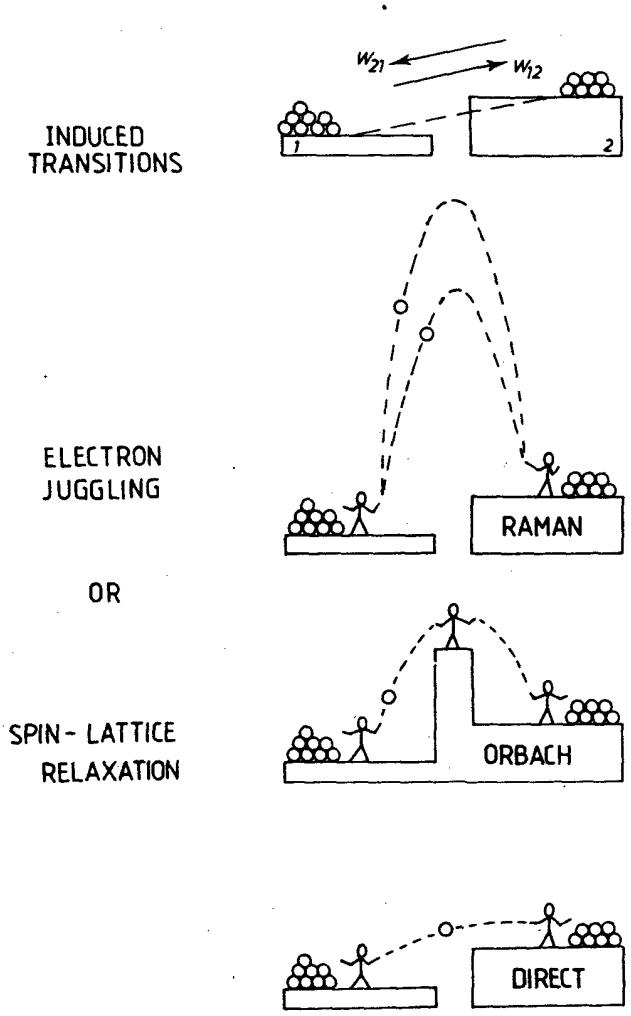

Figure 1. Simplified representation of induced transitions and spin-lattice relaxation time processes for an $S = 1/2$ ground state. Raman relaxation shows two of essentially infinite number of 'virtual' transitions.

metry allowed polynomials in the components of the electron spin **S**. H_{ligand} represents hyperfine interactions (including quadrupole and nuclear Zeeman interactions) for the i-th ligand nucleus. While **g** and **A** are usually called tensors, they should really be referred to as interaction matrices as explained in Chapter 15 of Abragam and Bleaney's book (1). Proper second rank physical tensors are found for the second order fine structure interaction, **D**, usually represented by the two parameters D and E, as well as for P.

Rudowicz (15) identifies three types of spin Hamiltonian : (i) *microscopic* (including the Abragam and Pryce version) (13, 14), (ii) *phenomenological* where one guesses the terms needed and (iii) *generalized* or group theoretical where all symmetry allowed terms are included. In all three cases, only those terms that satisfy full Wigner time reversal symmetry are allowed. That is one is restricted to terms of the form $S^{\alpha}I^{\beta}B^{\delta}$ where $\alpha+\beta+\delta$ is even (16).

It is worth noting that for copper EPR, a high proportion of papers still use expressions for principal g- and A-values based on either a crystal field model (17) or the Maki-McGarvey (1958) expressions (18). These expressions retain their utility because of their simplicity. The Maki-McGarvey expressions cannot be used reliably for cases like thiocarbamates or selenocarbamates because ligand spin-orbit coupling must be included explicitly (19).

In CW-EPR the system is disturbed from equilibrium only a little, and the steady state population differences between the levels are maintained by a combination of induced transitions, where the up and down transitions have identical probabilities, and spin relaxation processes. The spin lattice relaxation rate is found to have the following temperature dependence in a large number of cases (14, 20)

$$T_1^{-1} = aT + bT^n + c\Delta^3 \exp - \Delta/kT \qquad (2)$$

where Δ is the energy splitting between the ground doublet and a nearby excited state. T_1 is the spin-lattice relaxation time and a, b and c are factors that are essentially constant though a may be field dependent. Spin-lattice relaxation occurs because of the existence of various effective couplings between the electrons and the lattice phonons. *Eqn. (2) is the second important equation in EPR.* The lin-

ear term represents a direct process, whereby a microwave photon exchanges its energy with a single phonon. Raman processes involve energy exchange between a single microwave photon and two phonons whose energy difference equals the photon energy. For Kramers doublets, n = 9, for non-Kramers doublets, n = 7, for some iron-sulphur proteins, n = 5, and in other cases n = 6.5 (21). The final term, which has been exploited for heme proteins (22), cobalt (II) complexes (23) and cobalt-substituted enzymes (24) represents the Orbach process where the rate governing step is thermal activation to a nearby level, a distance Δ away. The Orbach process is also described as a resonant Raman process. These processes are shown schematically in Figure 1.

III. New Insights into EPR (S=1/2)

By taking into account the quantum mechanical transition probability and statistical mechanics of two levels i and j involved in a transition, and the unbalancing of the microwave bridge on passing through resonance, a single EPR transition may be described by the equation (2, 4, 5, 25)

$$S(B,\nu) = C\nu\eta Q_0|V_{ij}|^2 f(\nu - \nu_0[B],\sigma_\nu) \quad (3)$$

where ν is the microwave frequency, B the magnetic field, η the sample filling factor, Q_0 the unloaded quality or Q-factor of the sample resonant cavity, V_{ij} the quantum mechanical transition matrix element, f the lineshape function and σ_ν the linewidth in frequency units. At the magnetic field B, $\nu_0[B]$ is the resonant frequency between the eigenvalues E_i and E_j. *Eqn. (3), which is the third of the important equations in EPR, is a master equation by means of which both field- and frequency-swept EPR may be described.* Figures 2 and 3 illustrate some of the implications of equation (3).

Figure 2 contrasts the usual way of representing a two-level system (Figure 2A with Figure 2B) which highlights the frequency domain view of an EPR transition. In the latter, for simplicity, all of the linewidth information is contained in the upper level. In the usual field-swept mode $\nu = \nu_c$, the constant applied frequency, while $\nu_0[B]$ varies linearly with magnetic field via the resonance condition

$$h\nu_0[B] = g\beta B \quad (4)$$

On the other hand, frequency-swept EPR requires B fixed (or even zero). Therefore $\nu_0[B]$ is constant while ν varies across the line. The presence of ν in eqn. 3 implies that frequency-swept lines, as observed, will be asymmetric, and to obtain the shape function, f, S must be divided by ν. Figure 3 makes the simple point that the signal intensity at the line centre is independent of the sweep mode.

Until 1975 it had been assumed that the field-swept shape function, f, could be written as $f_B(B - B_0,\sigma_B)$. Provided the lineshape is symmetrical in both domains, then

$$f(\nu_c - \nu_0[B],\sigma_\nu) \quad (5a)$$

may be replaced by

$$\frac{h}{g\beta} f_B(B - B_0,\sigma_B) \quad (5b)$$

What this means is that the detected signal height at the line center is the same irrespective of which of the expressions is used, since any expression which describes the signal must have the same dimensions whatever sweep mode is used (See Figure 3). Eqn. 5b must be used with caution since the quantum mechanical transition probability used in eqn. 3 is an energy or frequency domain result. Such theory does not lead naturally to 5b. Computer simulation of EPR spectra should be based on eqn. 3. For a powder or frozen solution, where it may be assumed that the paramagnetic centers are randomly oriented in space, one may use the expression (26)

$$P(B,\nu_c) = \sum\sum\sum\ldots\sum S(B,\nu_c)\sin\theta\Delta\theta\Delta\theta \quad (6)$$

where the multiple summation implies inclusion of hyperfine, ligand hyperfine structure, isotope mixtures, etc.

For the necessary extension of eqn. 3 for $S \geq 1$ see the book by Slichter (25) and the paper by Coffman (2).

IV. Implications of Field-Sweep

A. Complications for S=3/2 (4)

The EPR spectrum of Cr^{3+} ions in ruby single crystals is well-known (27). At a number of microwave frequencies the angular variation of some spectral lines is somewhat unusual. For the so-called looping transitions, which occur between pairs of non-crossing levels, the lines become more and more

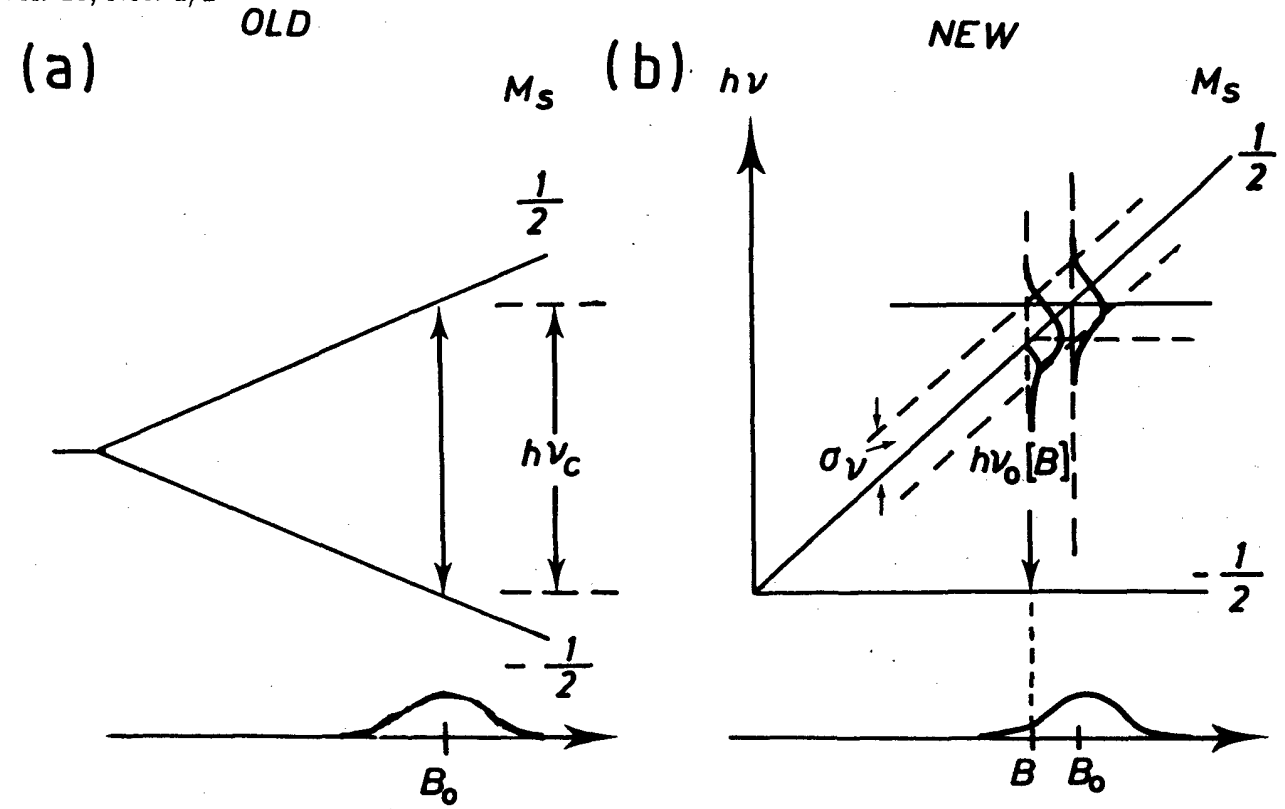

Figure 2. Old and new ways of understanding EPR. (a) implies use of eqn. 5b, (b) implies use of eqn. 5a. (Reproduced from ref. 6 with permission.)

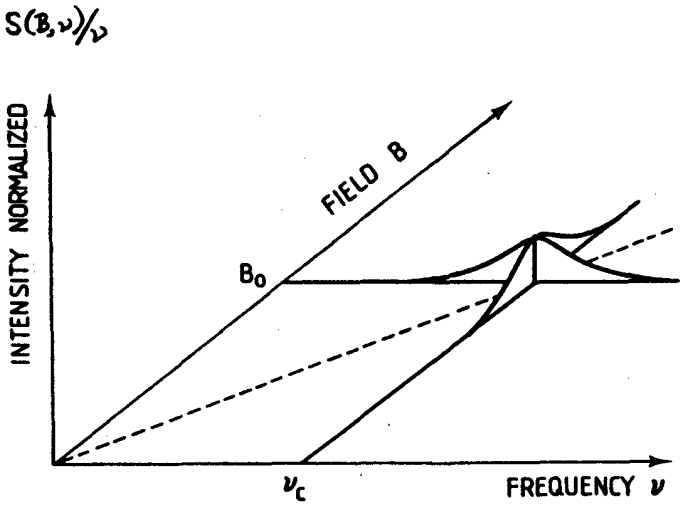

Figure 3. Single transition in both field- and frequency-sweep. Signal intensity at line centre has value independent of sweep mode. See text. (Reproduced from ref. 5 with permission.)

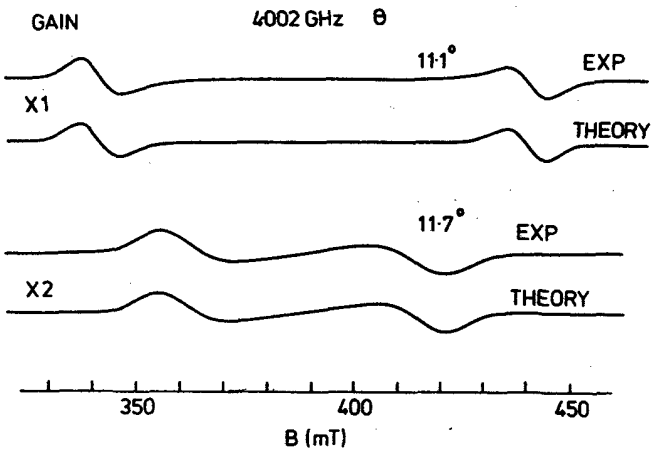

Figure 4. Part of the EPR spectrum due to Cr^{3+} ions in ruby at 4.002 GHz (28), recorded near the coalescence orientation for one pair of looping transitions. Simulation carried out using equation (3) and exact diagonalization of spin-Hamiltonian $H = g\beta B \cdot S + D(S_z^2 - S(S+1)/3)$ with $g = 1.985$ and $D = -5.747$ GHz. (Reproduced with permission from ref. 28).

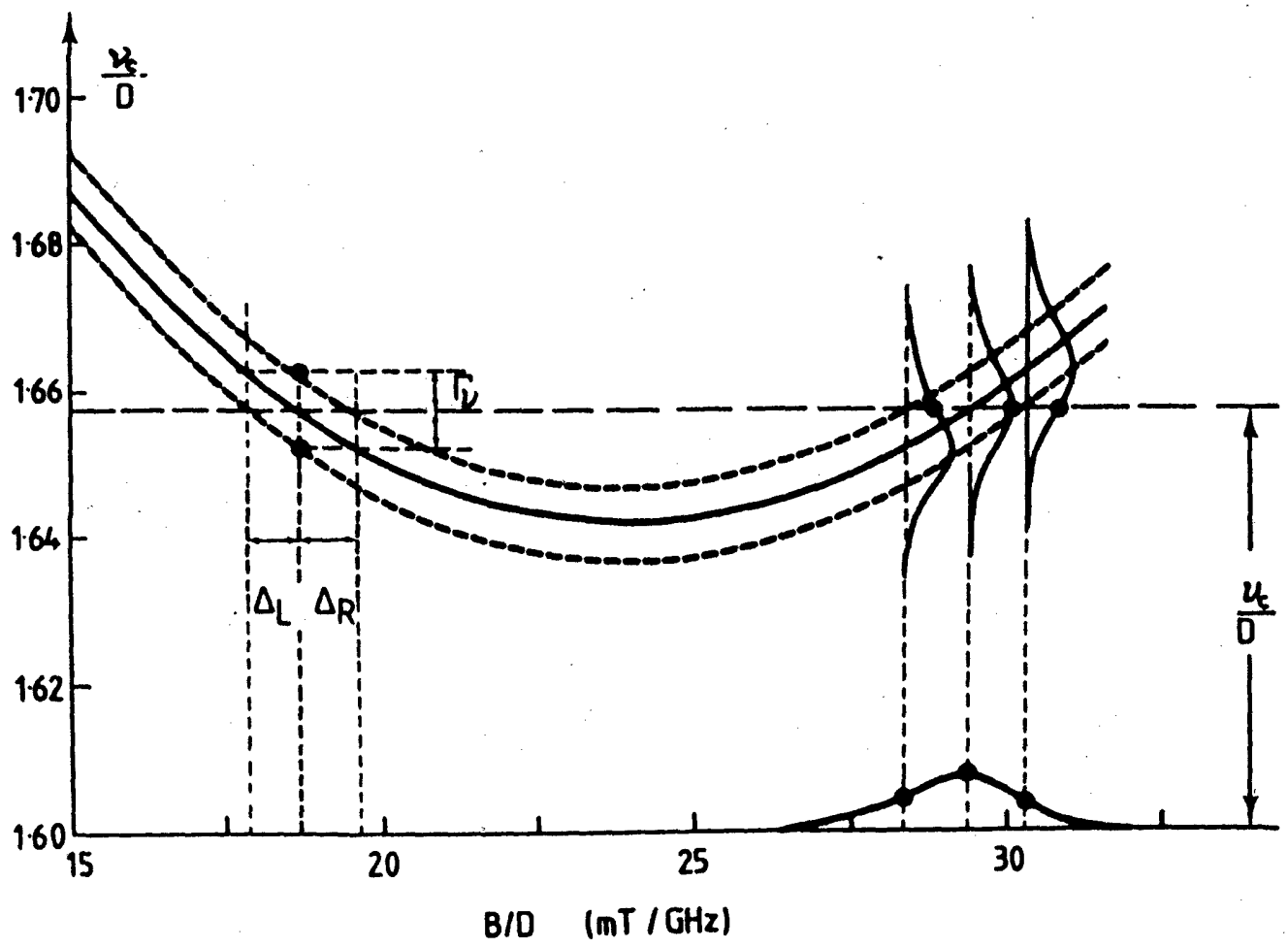

Figure 5. Relative energy spacing of the $\pm 1/2$ levels for Cr^{3+} in ruby (4) using reduced coordinates, $h\nu_0/D$ versus hB/D, when the c axis lies at an angle $\theta = 86.5°$ to the magnetic field direction, B (—). The half-width positions in the frequency domain are shown by the pair of – – – lines for the frequency domain shape function f (eqn. 3). Field domain widths for lower field line are Γ_L and Γ_R for left- and right-hand sides, respectively. In this figure f is assumed to be symmetric in frequency domain and to have constant width $\Gamma_\nu(\equiv \sigma_\nu)$ as B is varied. The fixed microwave quantum used at X-band is indicated by the horizontal (— — —) line at $h\nu_c/D$. Upper field asymmetric field-swept line sketched in bottom right hand corner. (Adapted from ref. 4 and reproduced with permission of journal.)

asymmetric as they move towards each other and coalesce. At about 9 GHz there are two such loops closing at $\theta \sim 28°$ and $\sim 86°$ from the c-axis. At 4 GHz there are also two loops, closing at $\theta \approx 12°$ and 42°, while at 2.9 GHz only one loop at $\theta \approx 33°$ is found.

Figure 4 (28) shows results observed at a microwave frequency of 4 GHz. Since first derivative lines are usually observed, they are marked by a loss of inversion symmetry through the cross-over point. Reference 4 gives the X-band results. The asymmetry arises from three different effects: (i) from repelling or non-crossing levels whose energy spacing is non-linear in magnetic field (see Figure 5), (ii) from transition probabilities which change by an order of magnitude over the spectrum and (iii) field dependent linewidths. All of these effects can be readily incorporated in eqn. 3; it would be rather difficult to carry out the simulations using the second of the lineshape functions in eqn. 5.

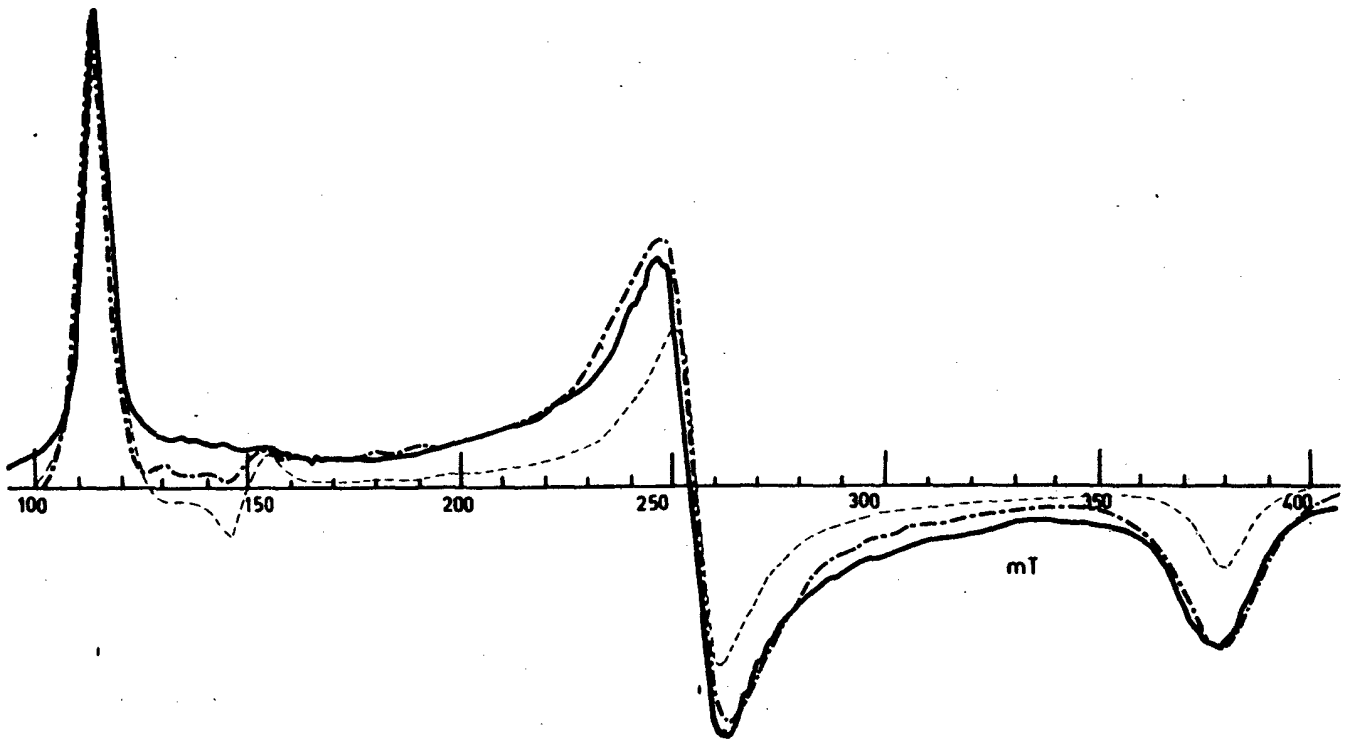

Figure 6. First derivative EPR spectrum due to cobalt(II) pyridine chloride powder (29). Computer simulated spectrum *with* (– – · – – · – –) and *without* (– – –) $1/g$ factor using older versions of our simulation routines based on eqn. 5b. An extra feature at 150 mT due to *algebraically correct* but *computationally inappropriate* algorithm for solid angles was removed from programs in 1980. (Reproduced from ref. 29 with permission of journal.)

B. Linewidth Anisotropy

While substantial levels of g-factor anisotropy are a common occurrence in transition ion EPR, the unusually high levels of linewidth anisotropy sometimes found appear hard to explain at first sight. Two examples are mentioned. The EPR of cobalt pyridine chloride powder has principal g-factors 5.82, 2.62 and 1.77 with corresponding widths in mT of 3.8, 8.0 and 12.0 (29) (see Figure 6). The products of $g\sigma_B$ are 21.2, 21.0 and 22.0 and are very nearly constant. A similar result is found for Nd^{3+} in lanthanum magnesium nitrate (30) where $g_{||} = 0.368$ and $g_{\perp} = 2.71$ with corresponding linewidths of 1.5 and 0.23 mT leading to the products of g and σ_B of 0.55 and 0.62. In other cases, especially where one of the principal g-factors is ≈ 0, not only does the corresponding linewidth become unmeasurable but the signal cannot be detected. Even so, it is found that the anisotropy in the product $g\sigma_B$ is always much less than in σ_B alone.

If we assume identical, symmetric lineshape functions in both domains, then since at the line center

$$\frac{h}{g\beta} f_B(0) = f(0) \tag{7}$$

then (5)

$$h\sigma_\nu = g\beta\sigma_B \tag{8}$$

The point of this argument is shown by Figure 7 for a case where $g_{||} = 2$ and $g_{\perp} = 4$, which is close to what is encountered for distorted tetrahedral high spin cobalt when $| D | >> g\beta B$.

In conclusion, the excessive anisotropy sometimes found for highly anisotropic spin 1/2 centers is in some cases completely, in others partially accounted for by the artificial anisotropy induced via the g-factors.

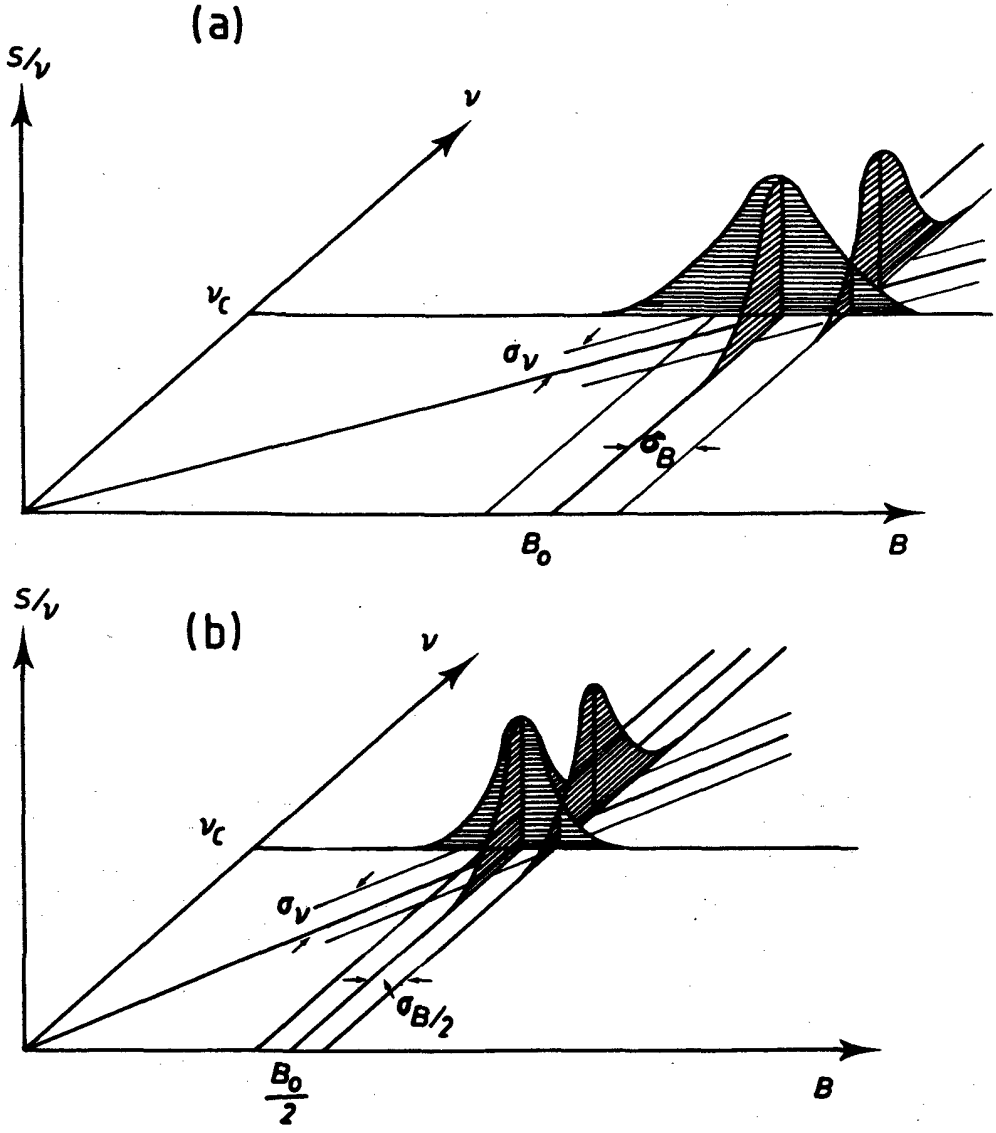

Figure 7. Relationship between field swept lines occurring in quite different parts of the spectrum, arising from an isotropic frequency sweep linewidth σ_ν. (a) $g_{||} = g_0$, width σ_B ; (b) $g_\perp = 2g_0$, width $\sigma_B/2$. Product $g\sigma_B$ is constant.

C. Introduction to Frequency-dependent or g-strain broadening

It has long been known that field-swept EPR linewidths due to transition ion complexes and metallo-proteins often show a pronounced increase in linewidth with increasing microwave frequency. In general terms, this has been attributed to a spread in the values of the g-factors caused by random strains (31). For spin 1/2, if the only source of line-broadening is that due to random strain, the resolution of the discernible features in the spectrum should be independent of the applied frequency. An example is shown in Figure 8 (32). Thus if

$$\sigma_\nu = c_1\nu_0[B] \qquad (9)$$

this should lead to the occurrence of asymmetric lines in field-swept EPR. In the case of a single line, the broadening should be more noticeable towards higher magnetic fields and the cross-over position of the first-derivative lineshape should move down in field (see curves in Figure 9 for increasing values of $c_1 = \Delta g/g$ where Δg represents the standard deviation in the distribution of the g-factor). Such

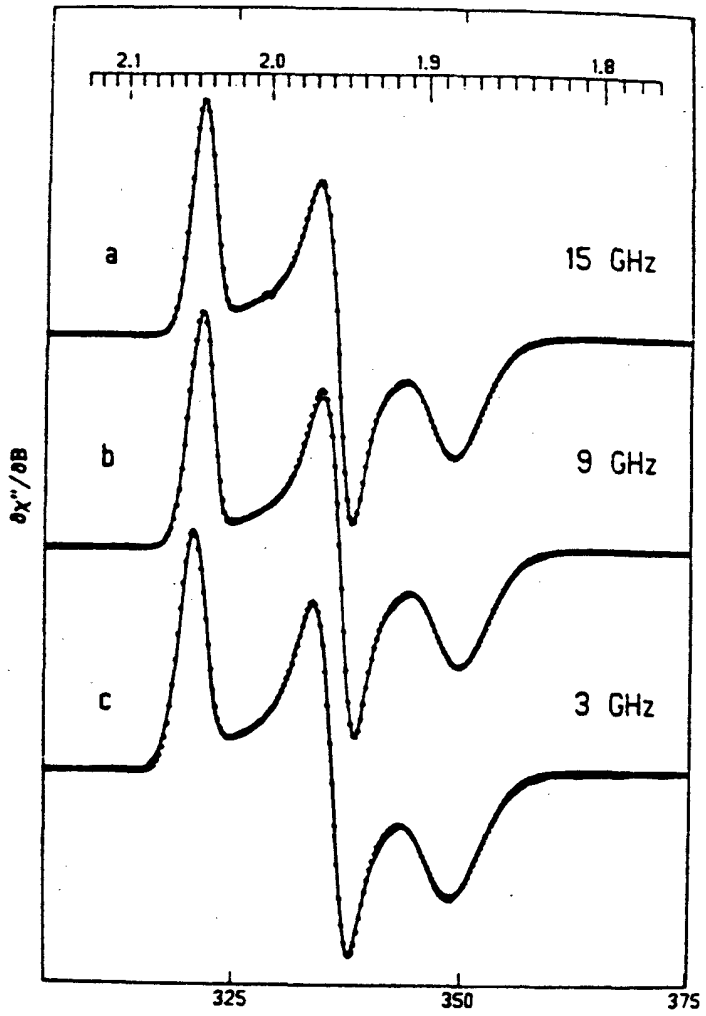

Figure 8. Experimental (solid trace) and simulated (dotted traces) EPR spectra, at three microwave frequencies, of the fully deuterated, ^{56}Fe reconstituted, reduced [2Fe-2S] ferredoxin from *Synechoccus lividus* (32). Microwave frequencies 14.975, 9.204 and 3.058 GHz ; microwave powers 0.12, 4 and 10 mW; modulation amplitudes 0.6, 0.1 and 0.4 mT; modulation frequency 100 kHz; temperatures 20, 22 and 22 K respectively. See ref. (32) for other parameters. (Reproduced with permission from ref. (32)).

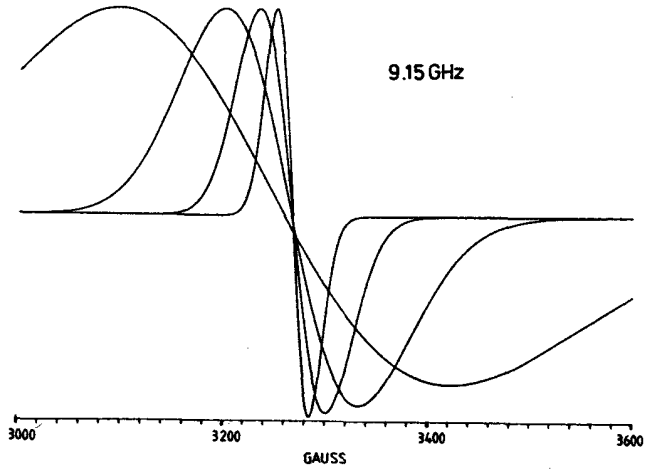

Figure 9. Computed '*g*-strain' broadened lines for c_1 = 0.0, 0.005, 0.01, 0.02 and 0.05 respectively, corresponding to the narrow to broad lines. (Reproduced from ref. (7) with permission.)

skewing of lines has been recognised for some time and the effect is automatically allowed for in some simulation programs (4-6, 25, 33-34). In the author's approach, no assumptions are made *a priori* about the field-swept lineshape, and its true shape is obtained naturally as a consequence of eqn. 3.

V. Low Frequency EPR

S-band (2 – 4 GHz) and L-band (1 – 2 GHz) EPR is now being carried out in many laboratories throughout the world. Microwave bridges, based on the design of Froncisz and Hyde (6) are readily constructed from commercially available coaxial microwave components and tunable solid state oscillators. The advent of loop-gap resonators (35-38) as revolutionized EPR at these lower frequencies because of the enhanced product of ηQ_0 where the improvement can be as much as 200 times at 3 GHz.

Improved resolution of copper EPR spectra at low microwave frequencies (39) is a strong motivation for such experiments. Figure 10 shows computer simulated spectra for copper(II) bound to transferrin. The X- and S-band cases may be compared with the original experimental data given in reference 39. Interesting results have been found for spectra due to molydenum complexes (40, 41) and for the molydenum-iron enzyme, xanthine oxidase (40, 42). In particular, for molydenum thiolate

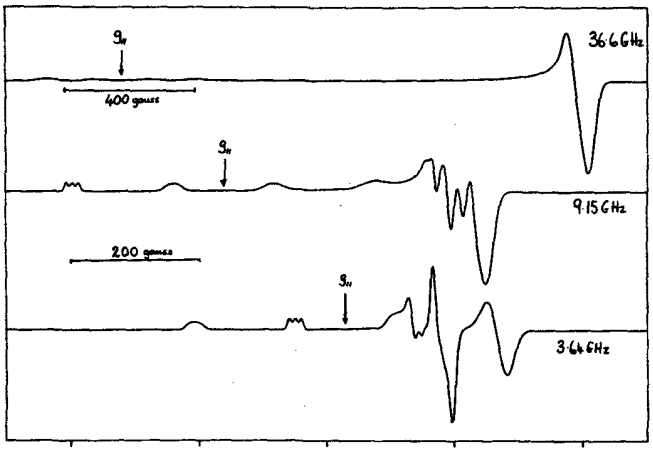

Figure 10. Theoretical simulations at 3.64 GHz, 9.15 GHz and 36.6 GHz for Cu^{2+} ($S = 1/2; I = /2$) in transferrin (7). The experimental spectra at 9.15 and 3.64 GHz are found in reference (39). The only parameter which is changed is the microwave frequency. (Reproduced from ref. 7 with permission.)

and selenate compounds, spectra recorded at 2, 2.9 and 4 GHz showed partially resolved ^{17}O and ^{77}Se satellites not observed at X-band (40, 41). Typical results are shown in Figure 11. The selenate examples are all the more noteworthy because naturally abundant ^{77}Se is only 7.5% abundant.

A test to distinguish between natural and synthetic sapphires has been developed using 2 GHz EPR by my colleagues D.R.Hutton and G.J.Troup (43) and takes about 5 minutes to perform. Results are shown in Figure 12. S-band EPR has also been found to be of value in the chemistry of technetium and rhenium complexes (44) and in resolving an old radiation damage problem in calcium oxide crystals (45).

Hyde and his colleagues have drawn attention to the factors which make low frequency EPR worthwhile (46). They include the $g - A$ strain effects in spin 1/2 spectra with hyperfine structure, state mixing and the consequent increase in intensity of forbidden transitions at L-band frequencies. In particular, experiments using parallel $\mathbf{B}$ and $\mathbf{B}_1$ fields select the forbidden transitions and thereby improve the precision of measurements of quadrupole interactions from frozen solution spectra. Rothenberger et al. (47) report such results for ^{63}Cu doped palladium bisacetylacetonate [^{63}Cu/Pd(acac)$_2$] where

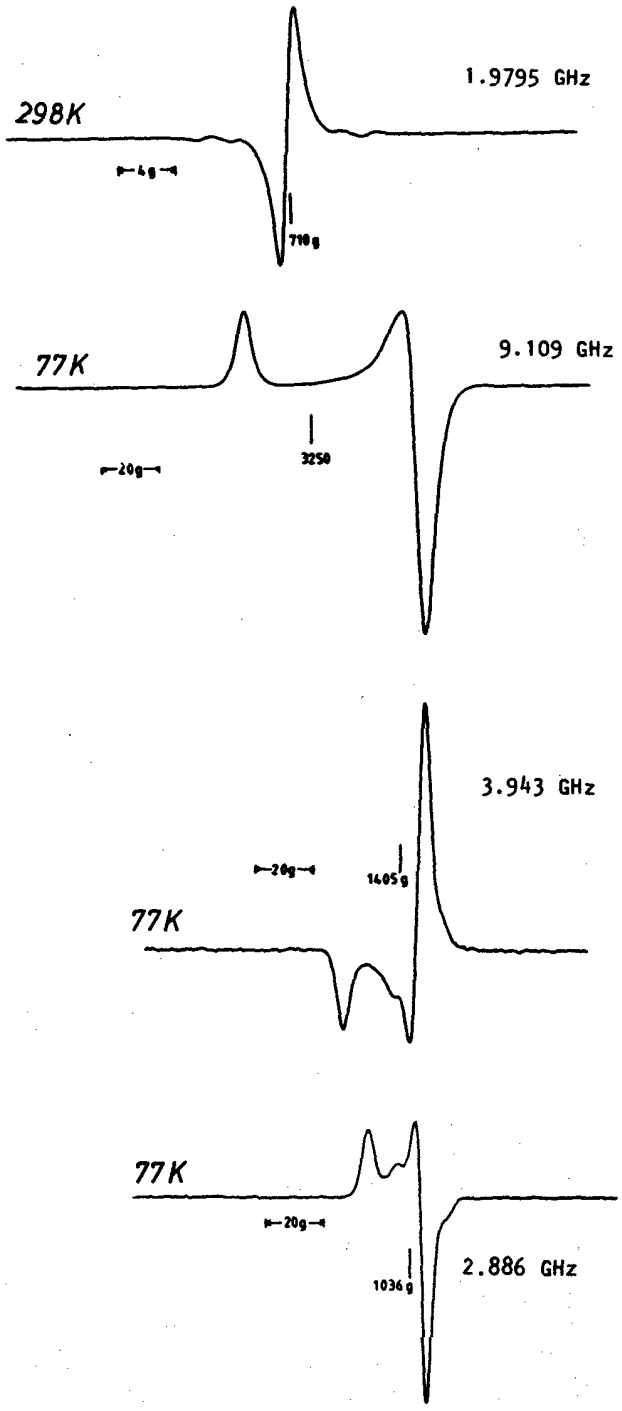

Figure 11. Multi-frequency EPR spectra of [^{98}Mo $^{17}O(SPh)_4$]$^-$ at 298 and 77K (40). Note appearance of satellites due to ^{17}O in 3 and 4 GHz spectra. (Reproduced with permission from ref. 40). For other examples, including simulations, see ref. 41.

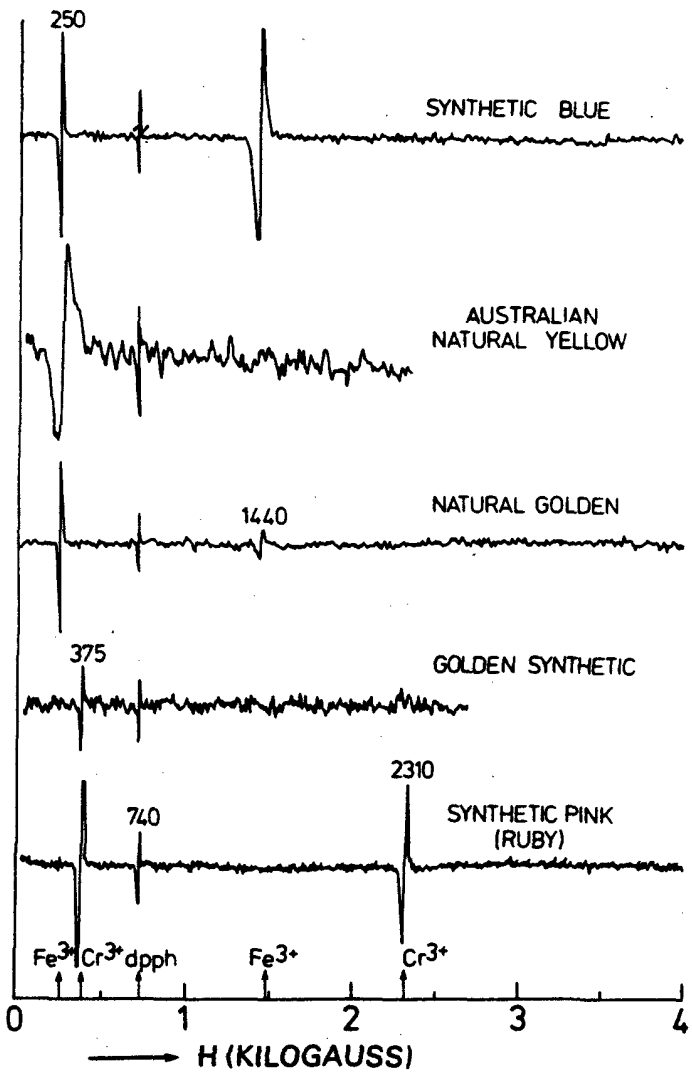

Figure 12. 2GHz EPR spectra of various sapphires: a synthetic blue, an Australian natural yellow, a natural golden, a golden synthetic, and a synthetic pink sapphire (43). Spectra are obtained by placing gem-stone in test tube which is inserted in large S-band cavity and rotated until the "⊥" spectrum appears at the turning directions. The golden synthetic is of more modern manufacture than those reported previously, shows no Fe^{3+} signal, and a very small Cr^{3+} signal in comparison with the other synthetics. (Reproduced from ref. 43 with permission of journal.)

the quadrupole constants were found to be $QD = 9\pm1$ MHz and $QE = 0.6$ MHz where QD and QE are analogous to D and E for second-order fine structure. The spacings of the forbidden peaks are found to be linear with QD. The notation for the quadrupole interactions is taken from that paper but other notations are found in the literature, e.g. P and R respectively.

Experiments at low microwave frequencies have provided the motivation for new and better simulation programs which can account properly for the various effects which determine the linewidths. In particular our experience has been that it is almost impossible to fit copper(II) or low spin cobalt(II) X- and S-band spectra for the same system with a unique set of linewidth parameters given the levels of modelling presently being used. This point will be discussed later.

A combination of S-Band EPR and computer simulations have enabled conclusions to be drawn about the binding of copper to the protein Bovine serum albumin. It has been established that the copper(II) ions bind to four approximately equivalent nitrogens (48). The simulations were sufficiently sensitive to the difference between three and four nitrogens that the result can be regarded as definitive.

Recently in Hyde's laboratory, a systematic multifrequency study of copper(II) histidine complexes has been reported both in the immobile phase (49) and in the mobile phase (50). Using a Monte-Carlo variation of parameters within defined limits, the best fit to the $m_I = -1/2$ parallel feature confirmed the presence of four equivalent nitrogens about the copper(II) ions.

In a recent review, Sealy, Hyde and Antholine (46) have outlined procedures which are worth following in order to expedite low frequency EPR operation. With copper(II) examples in mind, they recommended that single isotopes and deuterated solvents should be used wherever possible. They have found that at S-band using loop-gap resonators, satisfactory results are obtained from 1 – 5mM solutions of the copper complexes (51).

VI. Computer Simulations – Inclusion of Strain Broadening

The development of computer simulation programs for a variety of EPR situations has been of growing

importance during the past 20 years or so. More recently it has been necessary to improve the methods by means of which the following factors relating to linewidth are accounted for: (i) the variation of linewidth within a given set of hyperfine lines (m_I dependence); (ii) dependence upon microwave frequency and (iii) the idiosyncrasies of linewidth anisotropy.

Froncisz and Hyde (7) provided the basis for a consistent solution to (i) and (ii) above for a variety of copper complexes, finding nearly perfect correlation between $g_{||}$ and $A_{||}$. They established that the optimum frequency for resolving ligand hyperfine structure is in the 2 – 3 GHz range, and that the optimum resolution occurred for the $m_I = -1/2$ line. A particularly striking result is that for copper bound to transferrin there is only one bound nitrogen atom. The simulation (Figure 10), while not a perfect fit, illustrates the general principle. A careful reading of the literature shows that the frequency dependence of linewidths in copper spectra had been noted previously in the context of glasses (52).

For about four years the author and his group have employed a version of the Froncisz and Hyde model which has been expressed in frequency domain language consistent with eqn. 3. In this model the linewidth for routine calculations is based on the formula (26)

$$\sigma_\nu = \{ \sum_{i=x,y,z} [\sigma_{Ri}^2 + (c_{1i}\nu_0[B] + c_{2i}m_I)^2]l_I^2\}^{1/2} \quad (10)$$

where the σ_{Ri} (i = x, y, z) are the residual linewidths due to ligand hyperfine structure etc. and the c_1's and the c_2's are the widths of the g and A distributions. The l_i's are the direction cosines of the magnetic field with respect to the molecular axes. With this model it has been possible to obtain excellent fits to copper(II) and low spin cobalt(II) EPR for powder-like or frozen solution spectra at X-band but not, with the same input linewidth parameters, at ~3GHz. Sometimes the reverse is the case. This points to two factors. In the first place, the expression involving the c_1's and c_2's, eqn. 10, is correct only along the principal axes, for, as we shall see, the true orientational behavior depends, in general on direction cosines to the fourth power. It is possible to consider expressing the quantity σ_ν^2 as a sum of fourth order spherical harmonics. This has the consequence that for axially symmetric complexes such as porphyrins or porphyrazines, although g and A are axially symmetric, the full linewidth should reflect the true symmetry of the complex. Figure 13 shows both experimental and simulated spectra for cobalt(II) dibarreleno porphyrazine at X- and S-band frequencies. The actual simulations given here are based on the simple linewidth anisotropy using eqn. 10. The fit at X-band is satisfactory in this case where two axially coordinated nitrogen atoms are considered. There is a substantial variation in the widths of the cobalt hyperfine components especially for the perpendicular spectrum where an almost three-fold increase occurs from low to high field ends. It must be emphasised that the linewidths of each set of eight cobalt hyperfine lines along each principal direction in the molecule are governed by three parameters. Nevertheless, it is seen that the S-band results cannot be so accurately simulated with the same input parameters. In the next section a more rigorous model is considered.

Recently Hyde, Antholine and Basosi (51) have applied what they term a sensitivity analysis to multifrequency spectroscopy. It works as follows. A good fit is first obtained. Then that is compared with further simulations based on variation of one parameter at a time between defined limits. The statistical goodness of fit parameter is then plotted logarithmically against the parameter being varied for spectra computed at a number of frequencies (see Figure 14). It is found that the higher the frequency, the more sensitive the spectrum is to changes in g-factors; this is not altogether surprising! On the logarithmic plot, while the behaviour is independent of frequency, the actual changes at X-band are two orders of magnitude larger than those at L-band.

Continuing with the idea that the spin Hamiltonian parameters are random variables, certainly adequate for high symmetry, the linewidth variation for fully correlated g_i and A_i values, ignoring at this stage any correlation either amongst the g-factors themselves or amongst the A-values (53), may be written

$$\sigma_\nu = (\sigma_R^2 + \sigma_{gA}^2)^{1/2} \quad (11)$$

where

$$\sigma_{gA}^2 = \sum_{i=x,y,z} (\beta B\frac{g_i}{g}\sigma_{gi} + m_I\frac{A_i}{A}\frac{g_i^2}{g^2}\sigma_{gA})^2 l_i^4 \quad (12)$$

Here g and A are the values along the **B** direction (l_x, l_y and l_z) and σ_{gi} and σ_{Ai} are the standard deviations of g_i and A_i respectively. It is believed,

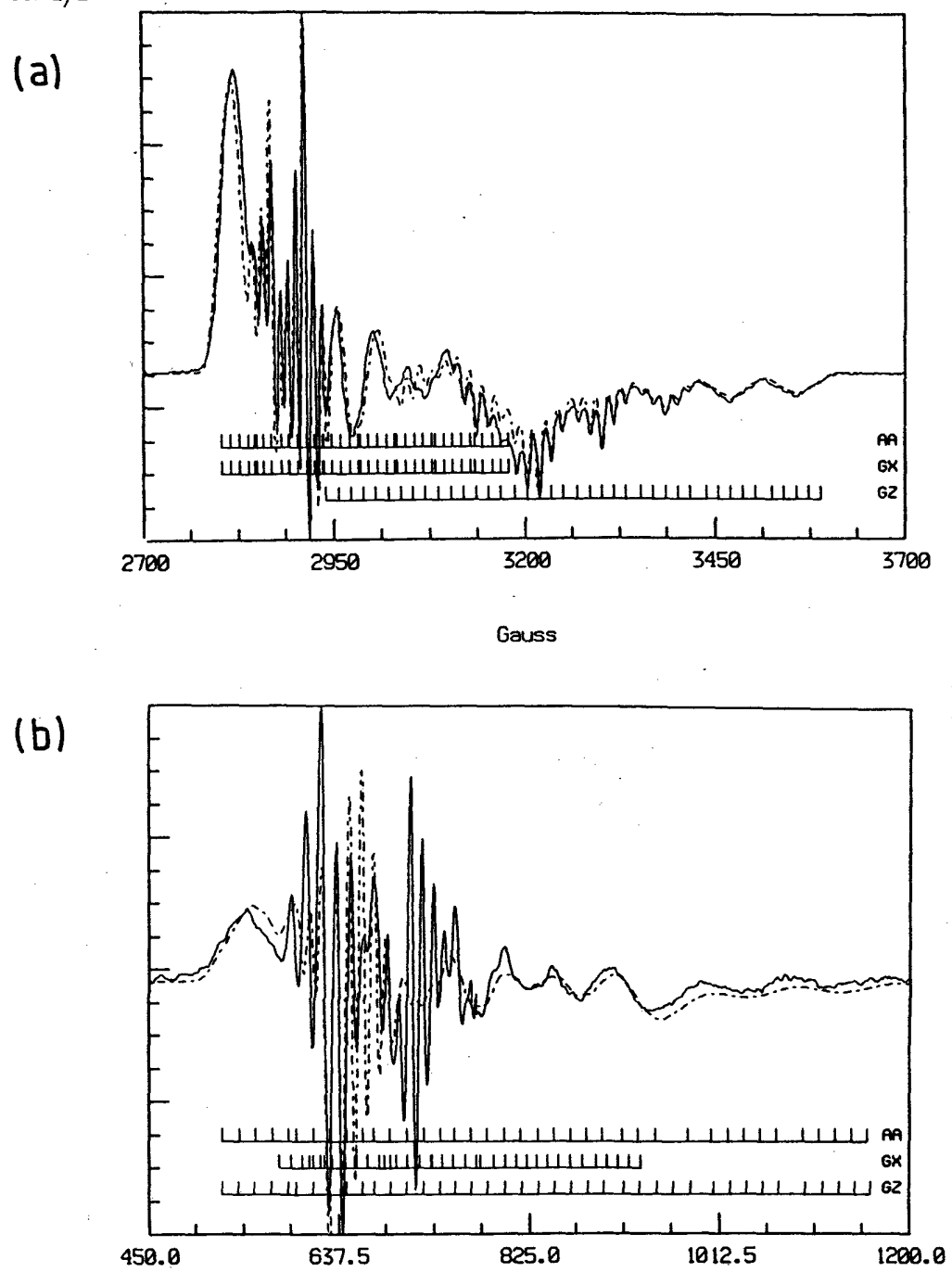

Figure 13. (a) X-band EPR spectrum at 9.115 GHz (—) and 120K due to a frozen benzene solution of tetra-(dibenzobarreleno)- porphyrazinato low spin cobalt(II) (1.0×10^{-3} M) containing pyridine (10% v/v) under dried nitrogen atmosphere. Computer simulation (- - -) with $g_{||}$ =1.986, $g_{\perp}$ = 2.179, $A_{||}^{Co}$ = 0.0078 cm^{-1} $A_{\perp}^{Co}$ = 0.0048 cm^{-1}, $A_{||}^{N}$ = 0.015 cm^{-1}, $A_{\perp}^{N}$ = 0.0012 cm^{-1}, $\sigma_{R||}$ = 8.5 MHz, $\sigma_{R\perp}$ =10.0 MHz, $c_{1||}$ = 0.00036, $c_{1\perp}$ = 0.0034, $c_{2||}$ = 5.8 MHz and $c_{2\perp}$ = 16.6 MHz; (B) Corresponding S-band spectrum (—) at 2.341 GHz. Computer simulation of spectrum (- - -) based on same linewidth parameters as for (a) but with slightly different g- and A- values reflecting the limitations of the perturbation theory solutions for the energy. Spectra recorded by Dr. S. W. Oliver (Ph.D. thesis, Monash University, 1986) and Figures prepared by G. R. Sinclair.

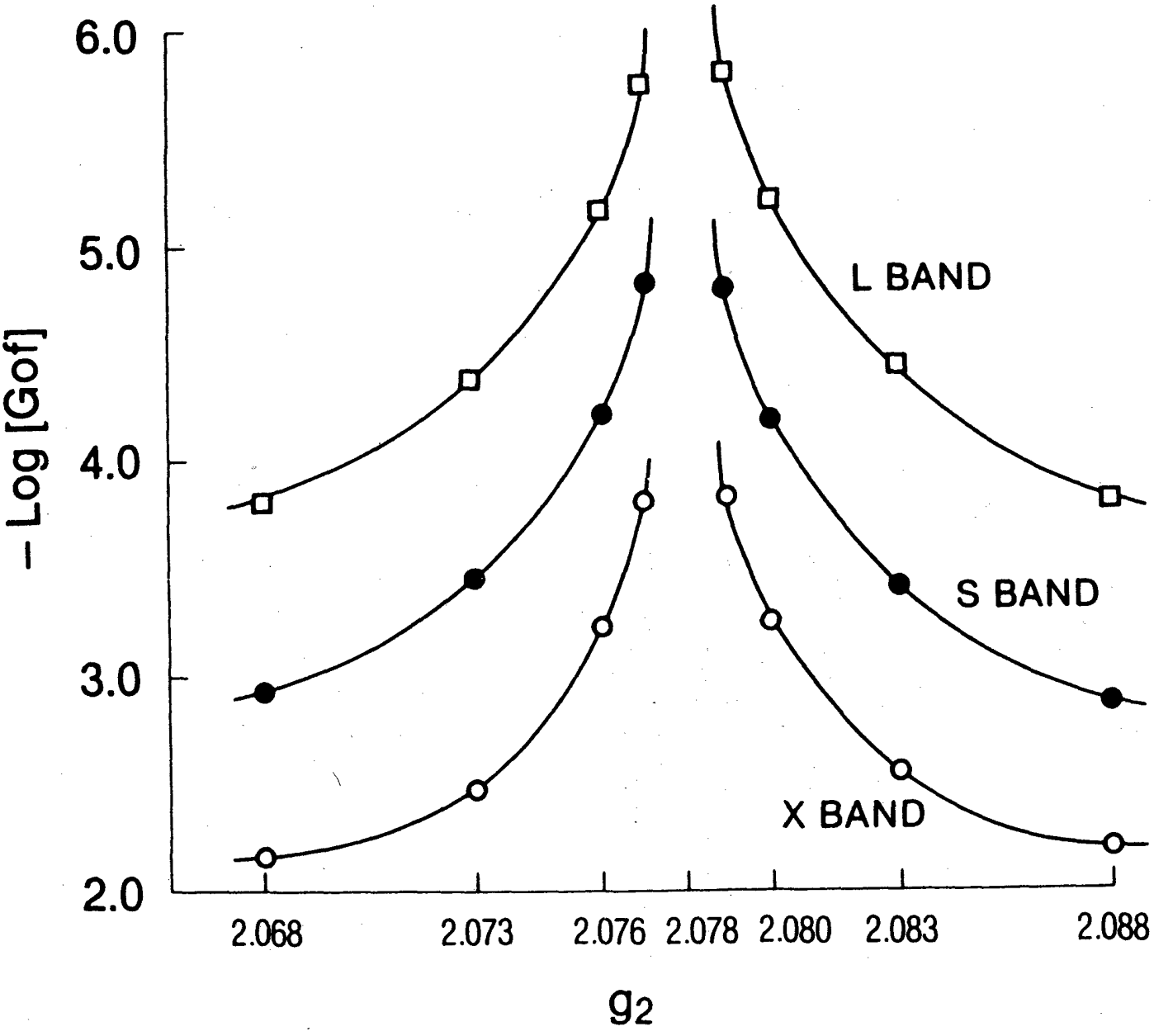

Figure 14. Goodness of fit verses g_2 for a copper (II) powder EPR spectrum ; $g_1 = 2.039$, $g_2 = 2.078$, $g_3 = 2.246$, $A_{||} = 0.0212\ cm^{-1}$, $A_{\perp} = 0.0030\ cm^{-1}$, linewidth 4 gauss. Values taken from Rist and Hyde, *J. Chem. Phys.*, **50**, 4352 (1969). Microwave frequencies: L-Band 1.2 GHz, S- Band 3.4 GHz and X-Band 9.1 GHz. (Reproduced from Figure 2 of ref. 51 with permission of the journal.)

even with this model, that the difficulty in fitting both X- and S-band spectra with the same linewidth parameters implies a field-dependence of the σ_R's. The residual width will include, amongst the various contributing interactions, unresolved hyperfine structure from protons and other nuclei belonging to the host and maybe even the solvent.

Calculations have been done by Brill's group for hemoglobin (54) using the Van Vleck moment method for dipolar broadening due to unlike spins

(55), which in this case are the metal ion and the various nuclei. In particular they calculated the proton contributions to the $g = 2$ linewidth for high spin Fe(III). This involved using the expression (54)

$$< \Delta\nu_A v^2 >= \frac{I(I+1)}{3h^2} \sum [g\beta g_n \beta_n (1 - 3\frac{\cos^2 \theta_{jk'}}{r_{jk'}})^2] \quad (13)$$

Such an effect should really be field dependent as the magnitude starts to become comparable to the hyperfine interaction at the lower S or L-bands where the effect of forbidden transitions should be more important. This is of special importance for protons with their large nuclear moments. It may not be entirely satisfactory, therefore, to treat these distant proton couplings by the Van Vleck method, since the Hamiltonian used to calculate the moments is truncated and field dependence is excluded. Eqn. 13 does, however, involve fourth-order Spherical Harmonics and may be a reasonable approximation to the full rotational symmetry of the linewidth at a particular microwave frequency.

In order to gain some insight into what Hagen et al (33, 34) have identified as zero strain directions in iron sulphur proteins, where the g-strain contribution to the width goes to zero away from principal g-axes, we have tried the following expression for the residual width as a linear combination of spherical harmonics of appropriate symmetry (56):

$$\sigma_R^2 = | \sum_{n \leq 4, m} a_n^m Y_n^M(\theta, \phi) | \quad (14)$$

Even for a high symmetry complex such as a porphyrazine (Figure 15), appropriate terms in eqn. 14, such as Y_2^0 and Y_4^0 give rise to small linewidths along non-canonical directions, and Y_4^4 has the four fold symmetry of the complex. In spite of this, agreement between X- and S-band simulations using the same set of input parameters still leaves something to be desired.

It is imperative that a model be found for which the g- and A-values are themselves functions of other random variables such as random strains entering via a spin strain Hamiltonian (57) viz.

$$H_{str} = \beta \mathbf{G} \cdot \epsilon \cdot \mathbf{B} \cdot \mathbf{S} \quad (15)$$

where G is the fourth rank spin-strain tensor and ϵ the strain tensor. The next section considers the effect of terms of this kind, but expressed another way.

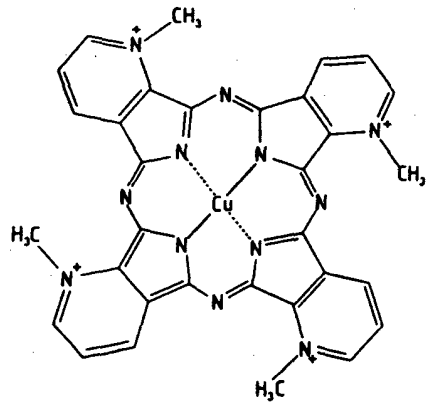

COPPER (II) TETRA (2,3-N-METHYLPYRIDYL) PORPHYRAZINE

Figure 15. Structure of Copper(II) tetra(2, 3-N-Methylpyridyl)-porphyrazine.

Dr. C. P. Keijzers (58) has drawn our attention to the occurrence of some previously unexpected orientational dependences of the linewidths for copper(II) in selenocarbamates. While the results have not yet been explained in detail, it is believed that they now can be understood in principle. For the systems in question, both ESEEM and ENDOR (59) data regarding distant nuclear interactions is known. Another example is the peculiar peculiar line broadening found for Cu^{2+} in ammonium chloride crystals (60) in orientations away from principal axes.

Hampton and Brill (61) also considered the crystalline state disorder, or mosaic, model of line broadening for high spin Fe(III) in heme proteins. The experimental data shows a very large change in width away from the two principal directions where the values are 24 and 30 gauss to a maximum of 400 gauss at a particular intermediate orientation (62). Fiamingo, Thorkildsen and Brill (63) considered the linewidth in the heme plane for high spin Fe(III) in hemoglobin and found it could be fitted to an expression for the square of the width (in gauss^2).

$$\sigma_B^2 = 159 - 22\cos 2\phi - 72\cos(4\phi - \beta) \quad (16)$$

where β is 122°. This is in accord with the earlier discussion relating to the symmetry of linewidth anisotropy for porphyrin-like molecules. More recently, Brill, Fiamingo and Hampton (64) have considered linewidth dependence of the $g = 6$ line due to alcohol complexes of ferric hemoglobin and myo-

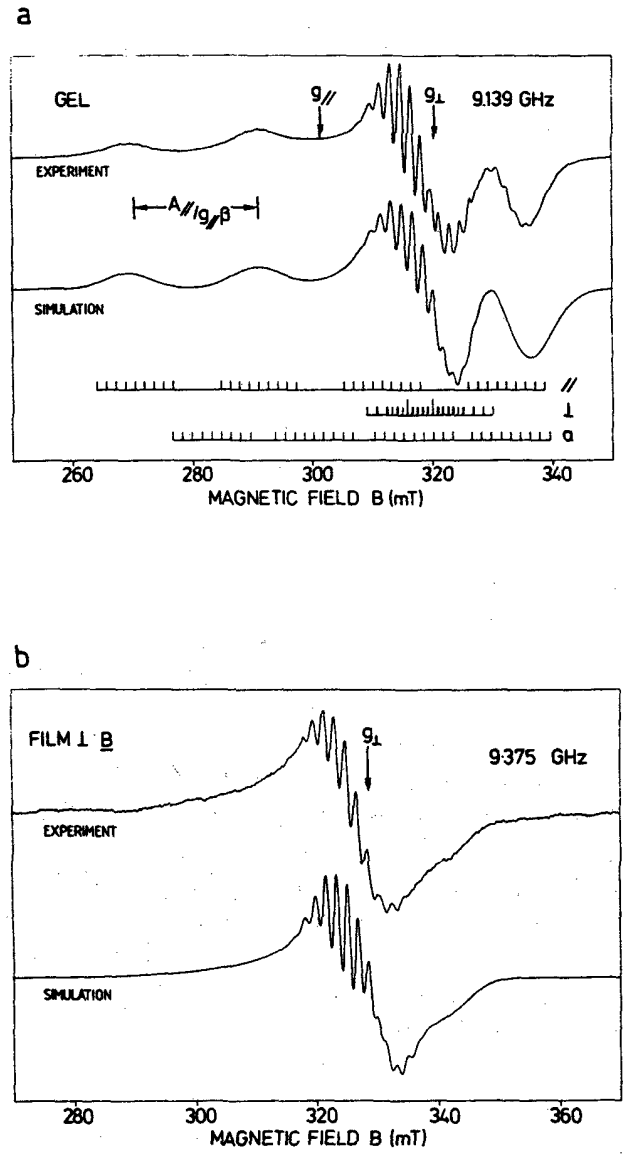

Figure 16. X-Band EPR spectra of copper(II) porphyrazine: calf thymus DNA (a) gel at ~110K and (b)gel-film at room temperature with **B** normal to film plane. Computer simulation of film spectrum uses modified program to allow for dye orientations in imperfect film. g- and A-values are typical of copper porphyrin and porphyrin-like compounds. Linewidth parameters: $\sigma_{R||} = 20$ MHz, $\sigma_{R\perp} = 9$ MHz, $c_{1||} = 0.010$, $c_{1\perp} = 0.002$, $c_{2||} = 16.7$ MHz and $c_{2\perp} = 1.9$ MHz. *See ref. 26 for other parameters.* (Reproduced from ref. 26 with permission of the journal.)

globin by considering the E/D ratio as the random variable.

A. Intercalation of Planar copper(II) complexes in DNA (26)

An interesting application of the EPR of planar copper and cobalt complexes to their binding to DNA, has been carried out in our laboratory for about four years now. It also raises interesting questions about linewidths, their true orientational dependence, and computer simulation of non-random distributions.

An EPR probe of intercalation in DNA must satisfy all or most of the following criteria. It should be planar, rigid and have non-trivial anisotropy and a room temperature EPR. Axial symmetry of the probe is ideal whereas orthorohombic symmetry may be too complicated. There is also the choice between using either oriented fibres or films. It has turned out that pressed films made by lightly compressing DNA-dye gels between two quartz plates are very reproducible. The experiments are easy to carry out and they discriminate, by inspection in some cases, between intercalated and outside-bound dye molecules. Intercalated molecules reflect the DNA fibre orientation while all molecules bound on the outside, or in the grooves, retain overall random orientation even in a 2D film of DNA fibres.

For copper(II) porphyrazine (Figure 15), even at low NaCl concentration (0.1M), all of the molecules are intercalated. Figure 16 compares the EPR spectrum of a DNA-dye gel and a pressed film with the magnetic field normal to the film. Clearly the low field parallel peaks have been suppressed in the film. In an ideal or perfect film, the latter spectrum should contain just the perpendicular spectrum. For copper porphyrins, similar results are found except that only with 1M NaCl in the original solutions is outside binding suppressed.

These examples are the more interesting because UV-visible binding studies show that the ratio of intercalated dye molecules to base pairs in calf-thymus DNA is 1:40, indicative of specific base sequence recognition; indeed it is likely that the dyes are specific to only three or four of the 130 different 4 base sequences.

There is another point to this example because of the much larger linewidths than occur for the porphyrins. The simulation, based on the simpler version of the Hyde-Froncisz model (eqn. 10), clearly does not describe the linewidths corresponding to

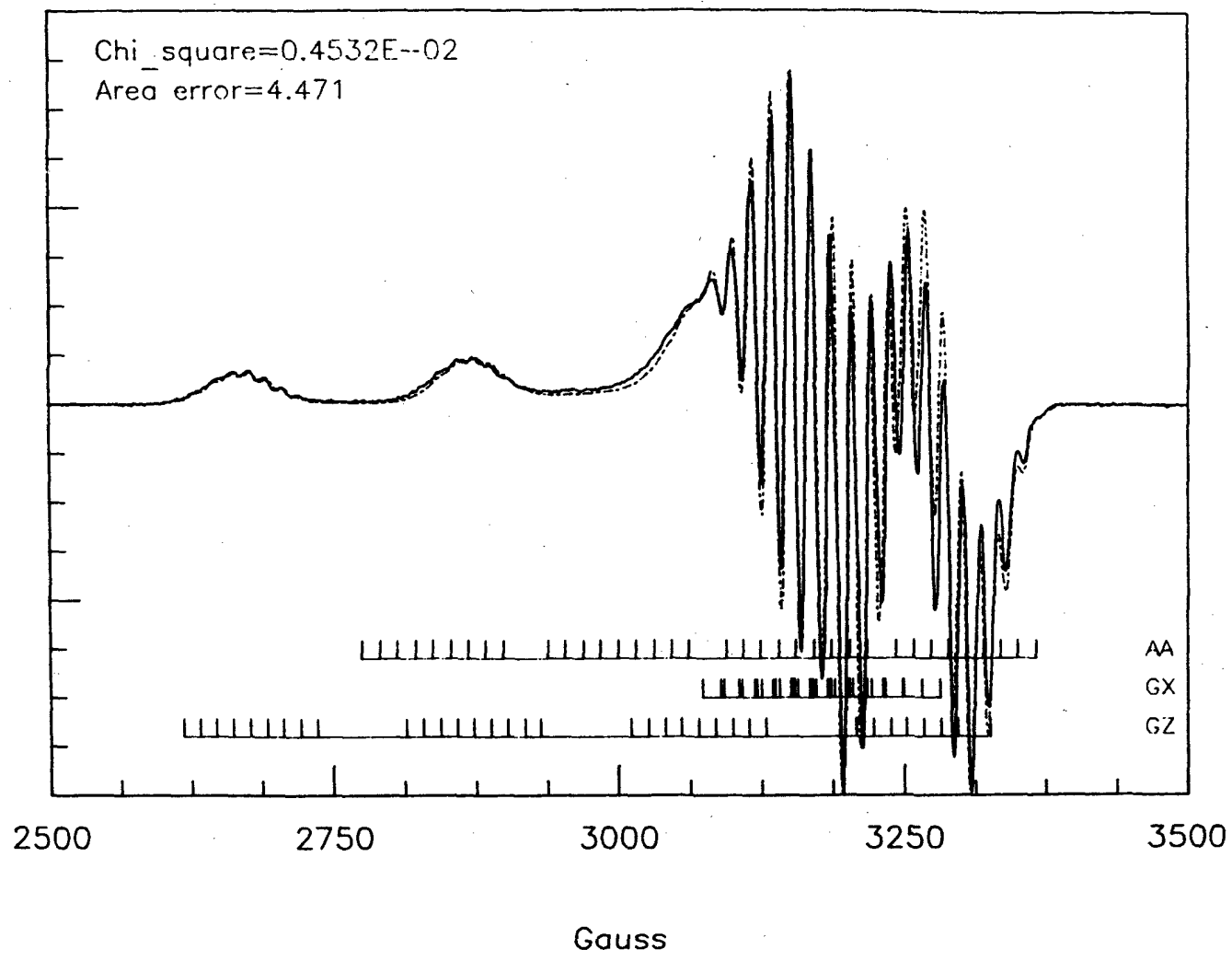

Figure 17. X-Band EPR spectrum of copper(II) porphyrin in 0.1M NaCl spun down to a gel. Microwave frequency 9.15 GHz. Spin Hamiltonian and linewidth parameters similar to those given in ref. 26. Note however that c_1 values for the copper (II) porphyrins in DNA are about ten times smaller here than for the porphyrazines (Figure 16). (Figure courtesy of Mr. Feng Yi).

the angular anomaly part of the high field feature. For the porphyrins, on the other hand, (Figure 17) (65) there does not seem to be the same problem.

B. Generalized *g*-strain Broadening

In this section the main points from some recent developments due to Hagen et al. (34, 35) regarding a generalized *g*-strain broadening model will be briefly summarized. In earlier work on iron-sulfur proteins, the authors had found that poor fits were obtained when the *g*-factors themselves were regarded as the random variables. What is described in the two papers by Hagen et al is an enlarged view of the problem. Much of the background to this work is to be found in an earlier paper by Hagen (31). A recent paper by Hearshen et al (32) applies the new theory to a rigorous assessment of data on given systems at three different frequencies (see Figure 8).

In this new model, the *g*-strain broadening is assumed to depend on a matrix p which parametrizes the strain induced linewidth information and which is separated from the static g matrix. The elements of p are taken to be the random variables, though

the precise origin of this randomness was initially unspecified. The g and p matrices do not, in general, share the same principal axes. This model is quite different from older simulation ideas where the lineshape was often regarded as little more than a useful smoothing function. The transformation between the g and p principal axes is defined by specifying the Euler angles between them. To cut a long story short, the expression for the linewidth, given here as the variance of g for a general orientation of the magnetic field, is

$$g^2\sigma_g^2 = \sum_{i=1}^{3} A_i l_i^4 + 2\sum_{j=i}^{3} B_{ij} l_i l_j^3 + 2\sum_{j<i} D_{ij} l_i^2 l_J^2 + 2\sum_{k\neq j\neq i} E_k l_i l_j l_k^2 \qquad (17)$$

where the $A...E$ quantities are complicated functions of the transformation matrix elements which are not needed in detail for this discussion.

A number of points need to be made. Hagen et al. (34, 35) work initially in terms of g- but their results could just as easily have been written in terms of ν. Eqn. 17 is in fact transformed to a 5×5 matrix representation for more compact computer programming. The important point to notice is that direction cosines of B w.r.t. g axes occur to fourth powers. Thus the angular variation of σ_g^2 (or σ_ν^2) depends on fourth order spherical harmonics as we have seen earlier. The detailed angular behaviour is expected to be very complicated with the possibility of zero strain directions for which σ_g is zero (32). Very efficient simulation algorithms were described including judicious use of Fourier Transform methods to filter noise in the simulations and to optimize the number of spatial orientations required. This is illustrated in Figure 4 of reference 35. An immediate consequence of their approach was that they were able to resolve a long-standing problem to do with the stoichiometry of the four iron- sulfur centres of NADH-reduced NADH:Q oxidoreductase and confirmed that it was 1:1:1:1. This provided them with strong ammunition for claiming that simulations require much more than a smoothing function in eqn. 3. These papers set a new standard for the quality of simulation necessary in chemistry and biology. The later paper by Hearshen et al (32) emphasises that a realistic computer simulations can be obtained via an ensemble of spin systems, each uniquely disturbed by it's own surrounding protein. They concluded on the basis of their analysis of EPR spectra that there are rigid inner regions and flexible outer regions in proteins.

C. Use of the Joint Density Function

A number of authors have tackled the problem of statistically based simulation models by using the joint density function for two random variables x and y (53)

$$f(x,y) = \frac{1}{2\pi\sigma_1\sigma_2\sqrt{1-r^2}} exp\{-\frac{1}{2\sqrt{1-r^2}}[\frac{(x-\eta_1)^2}{\sigma_1^2} - \frac{2r(x-\eta_1)(y-\eta_2)}{\sigma_1\sigma_2} + \frac{(y-\eta_2)^2}{\sigma_2^2}]\} \qquad (18)$$

where r is the correlation coefficient and η_1 and η_2 are the mean values of the random variables x and y.

The papers by Peterson et al (66, 67), describe a model for both Ti(III) and high spin Fe(III) in glasses where the random variables are assumed to be $g_{||}$ and $g_\perp$. In the latter case the aim was to see whether or not the characteristic g = 4 line in glass had an alternative explanation to the usual argument based on having E/D ≈ 1/3. Full positive correlation between the $< g_{||} >= 2$ and $< g_\perp > = 6$ values for high spin axial Fe(III) ground states did produce the required sharp feature at $g = 4$.

Cannistraro and Giugliarello (68-70) have written a number of papers relating to copper complexes where they consider the random variables to be $g_{||}$ and $A_{||}$. A high field shift of the parallel hyperfine peaks is reported which seems at first a little surprising since perturbation theories would lead to low field shifts and the largest spacing between the lowest pair. The reverse is found and accounted for by their simulations. It seems easier to understand the effect when the actual asymmetry in lines is allowed for, as is done in their later papers. This observation serves a warning about simply reading hyperfine values from spectra. Nowadays high level simulations are increasingly required for proper quantitative evaluation of EPR spectra.

It must be said that explicit use of the joint density function is useful when there are only two random variables. When there are more than two, it is clearly necessary to proceed as in the previous section, remembering, however, that the expansions used are approximations and require standard deviations of the random variables to be small.

The expressions in the papers by Giugliarelli and Cannistraro (69) for the goodness of fit are different from that used by Hyde et al (51) and reflect the fact that in EPR there is, as yet, no agreed definition. An important goal in EPR should be to seek a standard definition which would make comparison between the work of different authors somewhat easier.

D. Strategies for Powder/Frozen solution analysis

Here we turn to some of the possible strategies which can be helpful in evaluation of EPR spectra.

A first moment theorem was proved by Hyde and Pilbrow (71) for powder absorption spectra in the rigid limit. Application of the theorem leads to an accurate value for the mean g-factor $< g >$ and is potentially very useful for a 3 g-value problems. Estimates of g_1 and g_3, which can usually be easily obtained from the outer features of the spectrum, are combined with $< g >$ from the moment theorem to produce a good estimate of the intermediate g-factor, g_2. While the moment theorem was also obvious for rapid motion in solution, only recently have Pasenkiewicz-Gerula and Hyde (72) shown that it also holds, as was suspected, for slow motion in the liquid phase.

Belford and Pilbrow (73) showed that the usual assumptions about $< A >$ obtained from rapidly tumbling molecules in solution did not hold in low symmetry complexes where in order to specify **A**, more than three parameters are required. The motionally averaged value is not the mean value of the principal hyperfine values, but is actually Tr(**A**)/3.

Strategies actually employed in the analysis of copper(II) bound to four essentially equivalent nitrogens involve assumptions about the anisotropy in the nitrogen hyperfine interaction (26). To a first approximation one would expect that each individual ligand hyperfine interaction would be axially symmetric about the M-N directions, or even that it had three principal values. To keep the simulations tractable we assume that the values are isotropic in the molecular plane and that some variation can be allowed for along the symmetry axis. Since A^N values are, in general, relatively isotropic, this assumption is not too serious. Indeed the recent results of my student, Mr. Feng Yi (Figure 16) bear that out and represent about the limit of what can be done, short of a full numerical diagonalization of the energy, of which Belford's QPOW (76) programs (or our modification of it based on equation (3), QPOWFS) are but a first step.

Other strategies that ought to be considered for $S = 1/2$ are the use of Brillouin-Wigner (BW) perturbation theory which offers the prospect of more rapid and accurate convergence of energies than the more usual Rayleigh- Schrodinger (RS) theory. Thus one uses (76)

$$E_i = E_0 + V_{ii} + \sum \frac{V_{ij}V_{ji}}{E_i - E_{oj}} + \cdots \qquad (19)$$

My student, Mr. G.R. Sinclair, has carried out some trials in which a solution spectrum calculated using QPOWFS is taken as the reference. Then a perturbation theory simulation program was used where the energies were calculated using the Brillouin-Wigner expression (19). Secondly, by replacing E_i in the denominator of (19) by E_{oi}, the more familiar Rayleigh-Schrodinger form is obtained and a further simulation computed. The results obtained with the BW form, eqn. 19, to second order in the energies, are in far closer agreement with QPOWFS than are those using the RS version. The use of eqn. 19 is significant in that it fits in with eqn. 3 where the emphasis is on calculation of energy, or frequency, differences. Furthermore, it offers better quality simulations at low microwave frequencies.

It is noted that the Weil and Skinner (77-79) diagram methods provide complete and consistent expressions of perturbation theory.

E. Powder Simulations $S > 1/2$.

There is not space to go into any detail and it will suffice to list a few references to the papers by Coffman (2), Van Veen (80), Stevenson (81) and Korteweg (82). The papers by Van Veen and the Monash thesis by Kennedy (83) deal with the problem of the correct connection of the transitions as a function of orientation. It is noted that Coffman (2) based his simulation on the full expression for the absorption derived by Slichter (25), not the simpler form, eqn. 3, which applies to a two level system in the high temperature approximation. Scullane, White and Chasteen (84) use the Belford eigenfields approach for Fe(III) but in which no reference is made to Coffman's paper.

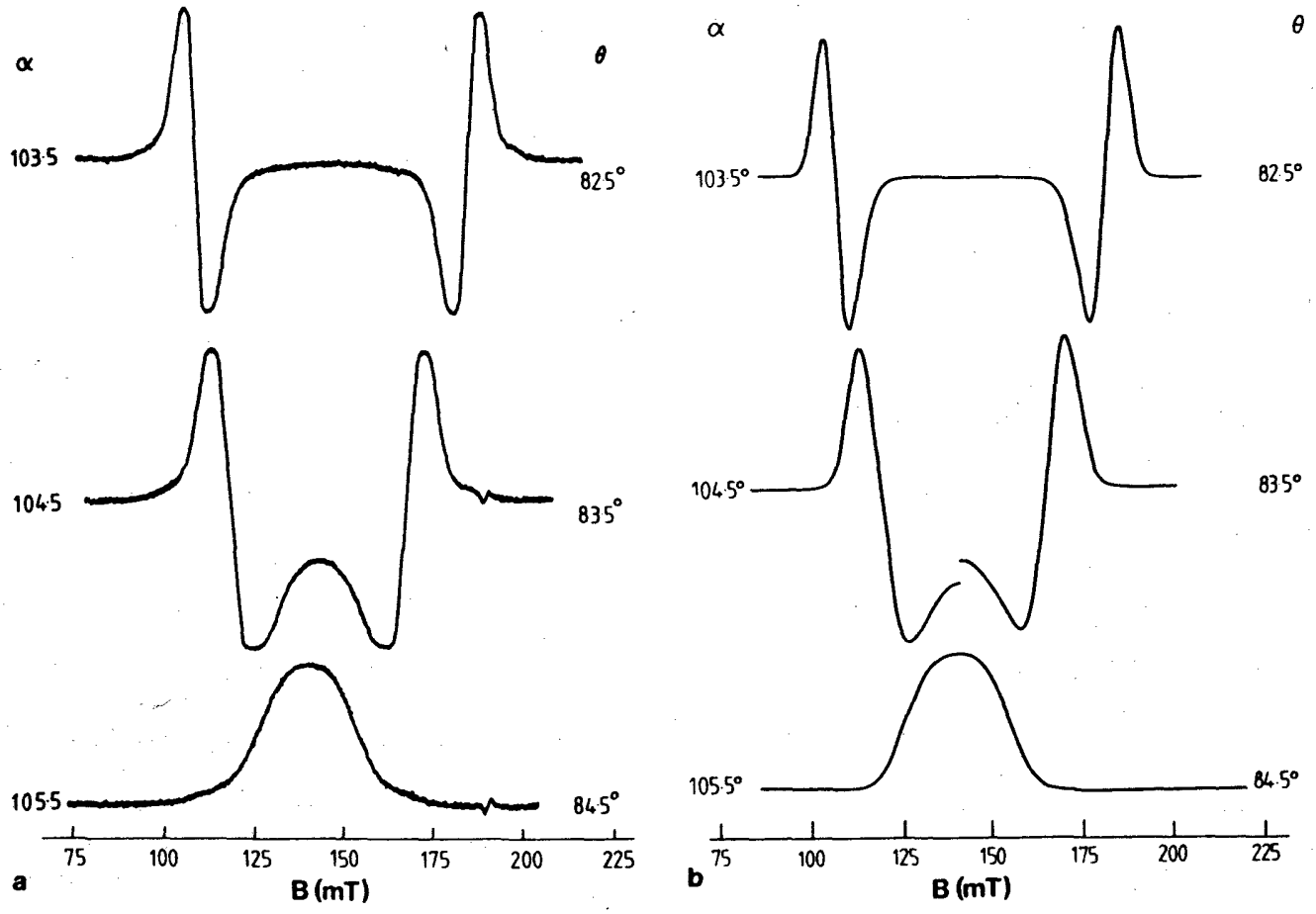

Figure 18. (a) Experimental angular modulated EPR spectra obtained at room temperature for "$\Delta M = 1$" "looping" transitions due to Cr^{3+} in ruby single crystals. Microwave frequency 9.240 GHz. (B) Theoretical fits to (A). Note the discontinuity when the lines overlap for the $\theta = 83.5°$ case. As explained in ref. (85), this discontinuity arises because different linewidths are used for the two transitions. (Reproduced from ref. 85 with permission of the journal.)

VII. Orientation and Angular Modulation – Site Selectivity

The author and his colleagues explained the occurrence of reverse phase lines in the EPR spectra of Cr^{3+} in ruby when there was a component of the modulation field normal to the d.c. field (85). The reverse phase effect is due to the dominant role of orientational modulation during a full modulation cycle. In those cases when the modulation field is normal to the d.c. field, then the spectral response is due entirely to the angular modulation effect. An example is given by Figure 18.

Schweiger (86) independently devised a related experiment in which the modulation field was circularly polarized and orthogonal to the d.c. field. Therefore, the resultant field rotates around the surface of a cone of angle ϵ (see Figure 19). In this experiment the phase of the resultant spectral response at the modulation frequency depends on which transition or site is being observed. In the illustrative example shown by Figure 19 we consider three axial sites in a cubic crystal where the symmetry axes lie along the crystal axes. With the d.c. field aligned along [110] the spectral responses are as shown. The spectra in the absence of the polarized orthogonal field are the normal perpendicular and 45° spectra EPR respectively. Upon application of the circularly polarized field, different orientations are sampled at different times in the modulation

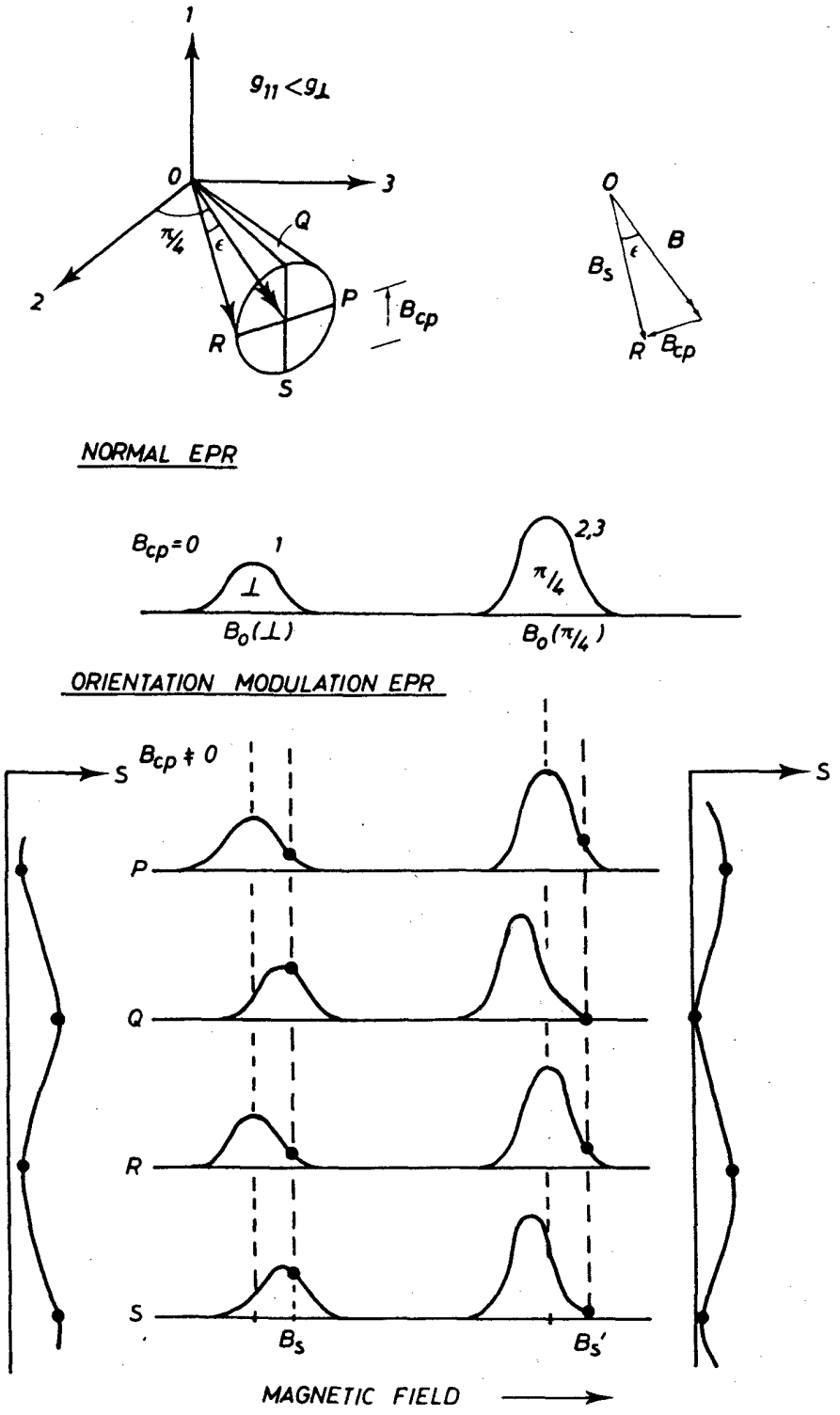

Figure 19. Schematic representation of a normal CW-EPR spectrum and orientation modulation EPR (OM-EPR) response during a modulation cycle. *Upper*: Resultant of d.c. field vector (**B**) and circularly polarized modulation field (B_{cp}) executes cone of angle ϵ. *Center*: Normal EPR spectrum due to axial centers in a cubic crystal with symmetry axes along cube edges. *Lower*: OM-EPR response over a complete modulation cycle showing nearly π phase difference. The first harmonic response (essentially first derivative spectra) will have opposite phases if PSD reference phase set to maximise either $\perp$ or $\pi/4$ spectra.

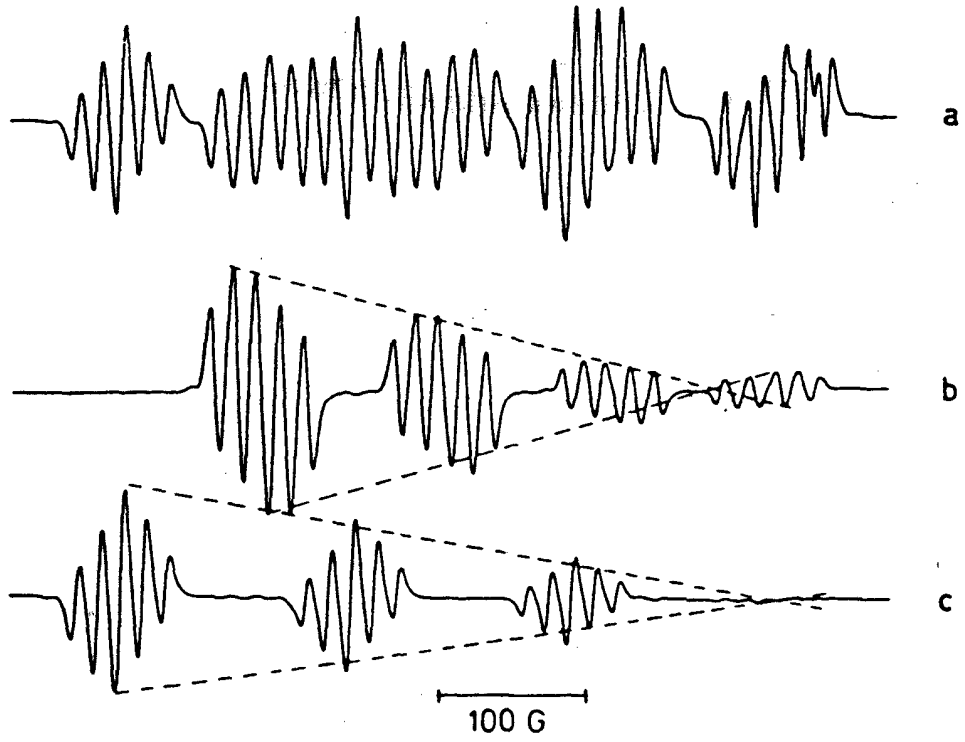

Figure 20. EPR spectrum of ^{63}Copper bisacetylacetonate [^{63}Cuacacen] diluted into Niacacen single crystal, arbitrary orientation, room temperature (86). (A) Conventional EPR showing overlapping spectra due to two sites. (B) OM-EPR spectrum of site I, phase of the PSD is 90° out of phase with respect to spectrum II. (C) OM-EPR spectrum of site II, phase of PSD is 90° out of phase with respect to spectrum I. Dashed lines in (B) and (C) illustrate dependence of the OM intensity on m_I. The reason for the lower intensity dependence on m_I towards the high field end is readily understood when it is realised that the high field hyperfine lines have much less orientational dependence than the lower hyperfine groups. Therefore the OM effect will be lessened. (Reproduced from ref. 86 with permission of the journal.)

cycle. The orientational modulation spectra in this case are out of phase with one another. By means of systematic variation of the reference phase angle in the PSD, spectra from different sites are enhanced or disappear at characteristic phase angles. Therefore one can use such experiments to identify spectra due to different centres and different sites (see Figure 20). The m_I dependence of the intensities can be understood by noting that the low field copper hyperfine component has considerably more anisotropy than the high field component in Figure 20 and is therefore expected to exhibit a much more marked angular modulation response.

Site selectivity can also be achieved using ENDOR-induced EPR (EI-EPR) where a particular endor transition is followed as a function of magnetic field (87, 88). This requires a computer controlled experiment as the ENDOR frequency must be altered in step with the change in the nuclear Zeeman interaction.

A less well-known experiment is that of ultrasonic modulation EPR (UMER) (Robinson and Devine (57)) where the crystal is mounted on the end of a quartz transducer oscillating at a frequency of about 40 kHz. Combined field modulation and UMER experiments make possible the enhancement of some lines at the expense of others.

In the absence of such techniques, the experimenter simply must undertake a systematic study of the angular behaviour of the spectra [e.g. Wang et al (89, 90)] or for spin 1/2, use of automated methods such as described many years ago by Waller and Rogers (91).

For $Cr(CN)_6^{3-}$ complexes in KCl (89) and KBr

(Figure 21) where the E/D ratio is very close to 1/3, some unsuspected symmetry relationships are found (90). Figure 22 depicts the situation for $S = 3/2$ spectra when g is isotropic; the surfaces indicated define orientations corresponding to different values of $\lambda = E/D$ for which the transitions between the two upper and the two lower energy levels are exactly superimposed. There is a common superposition orientation for all values of λ when g is isotropic.

VIII. Effective g-Factors for S=3/2

When the zero field splitting is larger than the microwave energy, such transitions as are observed in EPR occur within each of the two Kramers doublets (29). High spin cobalt(II) in nearly tetrahedral environments fit into this category and examples are found in a variety of inorganic compounds and also cobalt substituted carbonic anhydrase and carboxypeptidase A. Modelling of the electronic structure has been carried out using the angular overlap model (93). This work confirmed what had long been suspected that the g-factors, by themselves, do not provide adequate discrimination between four, five and six coordination. High spin cobalt complexes which are six, and sometimes five coordinate, show cobalt hyperfine structure, but this cannot be regarded as foolproof. It is found that hyperfine structure is not always seen observed for the cobalt substituted enzymes (94a, b).

The theory which the author brought up to date in 1978 (29) has been extended, showing that the ratios of the effective g : A values for each principal direction for both upper and lower doublets are identical to the true values:

$$\frac{A_i}{g_i} = \frac{A'_{ui}}{g'_{ui}} = \frac{A'_{li}}{g'_{li}} \qquad (20)$$

where i = x, y, z and where the $'$ components belong to the upper (u or $\pm 3/2$) and lower (l or $\pm 1/2$) doublets. Eqns. 20 convey the gist of the detailed AOM calculations (93) and this is borne out by noting the similar dependences shown by Banci et al. (93) for the corresponding g' and A' values of upper and lower doublets as functions of the AOM parameters.

Hagen and his associates at the University of Michigan and the Agricultural University of Wageningen have considered some novel spin 3/2 spectra due to native Fe proteins of nitrogenase (95),

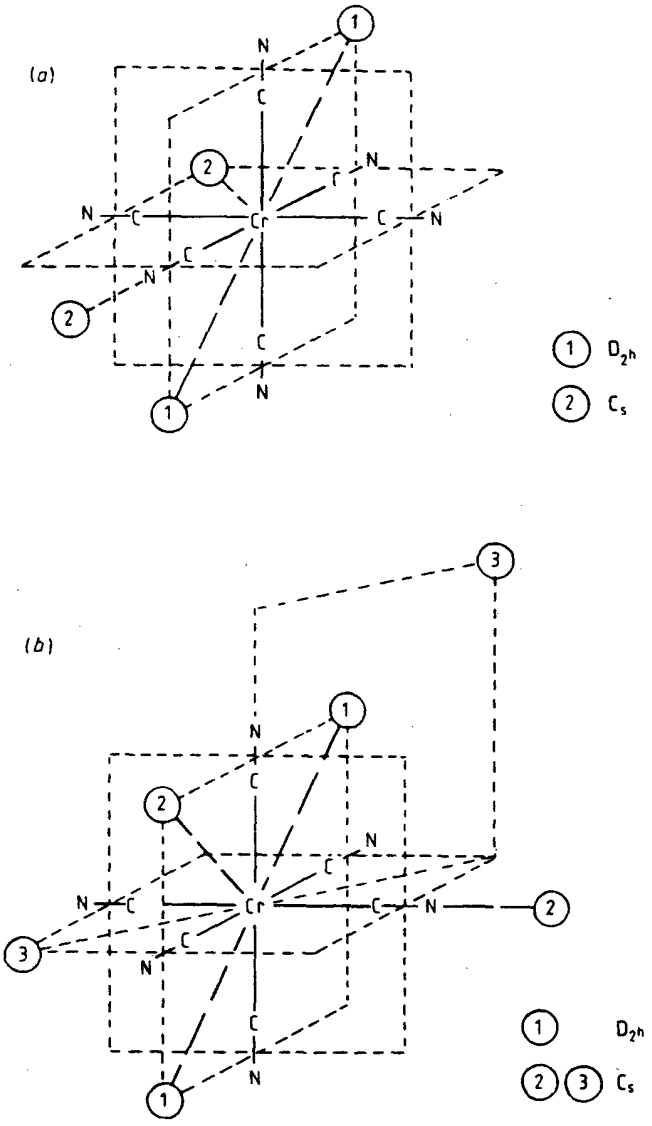

Figure 21 (89). (A) Two charge compensating vacancy configurations previously reported for some trivalent metal cyanide complexes doped into alkali halide crystals with the two point symmetries D_{2h} and C_s. (B) Possible charge compensating vacancy configurations for center I and center II of $Cr(CN)_6^{3-}$ in KCl. (Reproduced from ref. 89 with permission of the journal.)

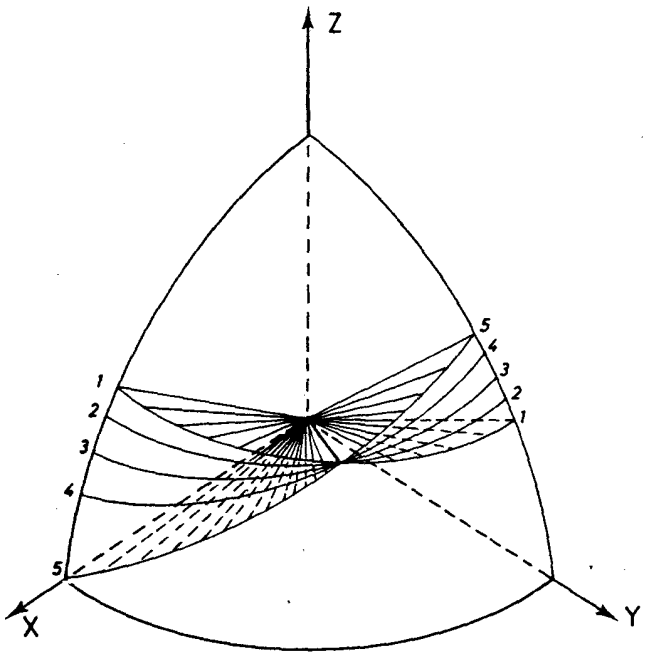

Figure 22. Schematic of surfaces of coalescence of transitions between upper and lower pairs of levels for $S = 3/2$ when g is isotropic for different values of λ (91). $\lambda = 0$ corresponds to 1, λ =1/3 to 5. Common orientation occurs only when g is isotropic. These surfaces are not based on a full numerical calculation and are meant to be illustrative only. (Reproduced from ref. 91.)

which catalyses the ATP-dependent reduction of nitrogen to ammonia. In addition to the g = 1.94 signal, nitrogenase proteins from Azotobacter vinelandii and chrococcum and Klebsiella pneumoniae have effective g factors for the $\pm 3/2$ doublet $g_z = 5.9$ and for the $\pm 1/2$ doublet $g_x = 4.8$ and $g_y = 3.4$. The fine structure parameter, D, corresponding to the full $S = 3/2$ ground state has the value -5 ± 0.7 cm^{-1}. There is a single [4Fe–4S]$^{(2+,1+)}$ cluster in the Fe protein whose principal g-factors are 1.85, 1.94 and 2.06. For the MoFe subunit, D was determined from the temperature dependence of the spectra. What is surprising about these results is that unlike cobalt carboxypeptidase A, where Orbach relaxation causes a loss of the signal above about 15K, this does not appear to happen here. Presumably this has to do with the particular phonon modes responsible for the relaxation.

Lowe and Smith (96) also report results for nitrogenase and although they find the same value for the zero field splitting at 15K they report the opposite sign!

IX. Non Kramers Ions and Non Kramers Doublets (97)

EPR spectra have been reported for even electron ions with characteristic sharp edges and cut-off magnetic fields (98, 99). Similar strange shapes are found for non-Kramers ions measured by acoustic paramagnetic resonance(APR) (100) and thermal detection EPR(TD-EPR) (101). In conventional EPR experiments transitions are strongest when $\mathbf{B} \| \mathbf{B}_1$ and forbidden when $\mathbf{B} \perp \mathbf{B}_1$ when $S = 1/2$. The theory for the lineshape by Baker and Bleaney (98), repeated in the book by Abragam and Bleaney (1) and again in an article by Williams (99) is not correct at the point at which the calculated expressions are transformed into field variables. It turns out that the model, in its simplest form, also runs into a problem in regard to transitions induced by microwave electric fields. This is because of a factor in the denominator which goes to zero at the cut-off field but which was not included in the original theory.

The energy levels in zero and low magnetic fields for the case of $S = 2$ considered by Abragam and Bleaney, are shown in Figure 23A. The zero field splittings (zfs) of the levels are 6E and $3E^2/D$ and are represented by Δ. In the near axial limit, but

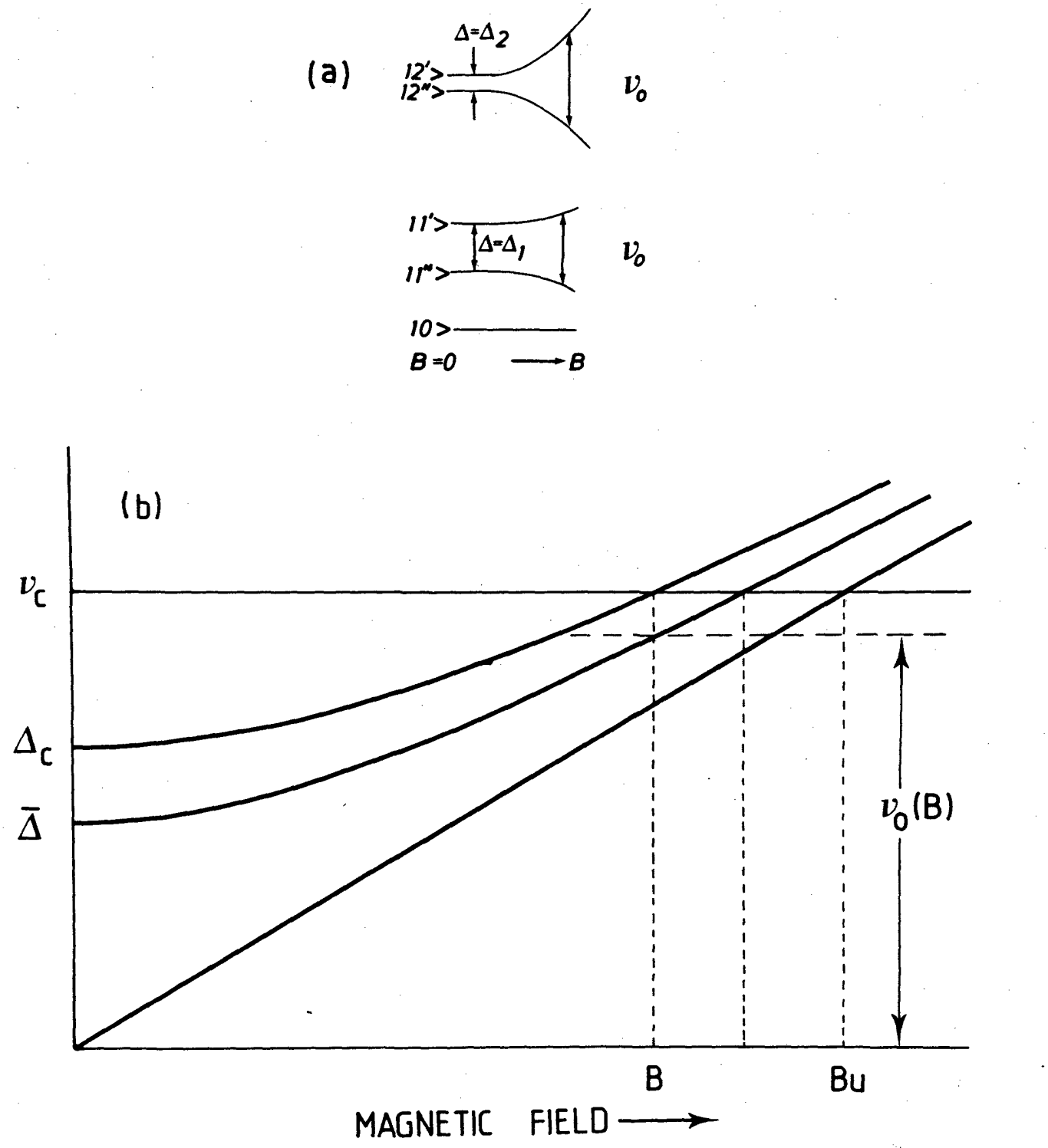

Figure 23. (A) Schematic diagram showing the behavior of the $|0>$, $|\pm1>$ and $|\pm2>$ levels with increasing magnetic field. (b) The $|\pm1>$ levels in frequency units, with all of the field dependence shown in the upper level. ν_c is the fixed microwave quantum. In a field swept experiment, resonance occurs at B when $\Delta = \Delta_c$. For the upper energy level, zero field splitting is Δ_c; for the mean energy level, the zero field splitting is $\bar{\Delta}$; when $\Delta = 0$, $\nu = g\beta B$.

where random fluctuations in symmetry result in random variations in E, the level diagrams relate to a particular value of Δ. In the model it is assumed that if the E values are normally distributed about a mean value $< E >$, with a standard deviation E_o, then the probability distribution in E is given by

$$P(E) = \frac{1}{\sqrt{2\pi}E_0} exp - \frac{(E - < E >)^2}{2E_0^2} \qquad (21)$$

Figure 23B shows schematically the field-dependent behavior of the energy levels for a given zero field splitting. For the $| \pm 1 >$ states the zero field splitting is linearly related to E so it too will be randomly distributed about a mean value $< zfs >$ which can be zero. For the $| \pm 2 >$ levels one must base any lineshape theory directly on use of eqn. 21.

$\mathbf{B_1}$ along the molecular symmetry axis and $\mathbf{B}$ and $\mathbf{B_1}$ making an angle θ with each other, the transition probability is proportional to

$$|V_{ij}|^2 = \frac{\Delta'^2}{(g_{||}\beta B \cos\theta)^2 + \Delta'^2} = \frac{\Delta'^2}{\nu_c^2} \qquad (22)$$

The limiting zero field splitting occurs at the cut-off field, B_u, when

$$\nu_c^2 = g_{||}\beta B \cos\theta \qquad (23)$$

From the relation

$$\Delta_c^2 = \nu_c^2 - (g_{||}\beta B \cos\theta)^2 \qquad (24)$$

it can be seen that there are two valid solutions for Δ_c. The total spectral response must be the sum of these two contributions which become identical when $< E >= 0$.

The equation equivalent to 3 in this case is (97)

$$S(B, \nu_c) = K\nu_c \frac{g_{||}\Delta_c^2}{\nu_c^2} \{ \frac{1}{\sqrt{2\pi}E_0}$$

$$exp - \frac{(E - < E >)^2}{2E_0^2} | \frac{dE}{d\nu} |_{\nu_c} \} \qquad (25)$$

The $|dE/d\nu|$ term is necessary to put eqn. 25 in the form required by eqn. 3. For both doublets, the magnetic field induced transitions lead to the result that $S(B, v_c)$ is proportional to E. Figure 24 shows calculated spectra for the $| \pm 1 >$ doublet and the results may be compared with the original spectrum for Pr^{3+} in yttrium ethyl sulphate [Baker and Bleaney (98)].

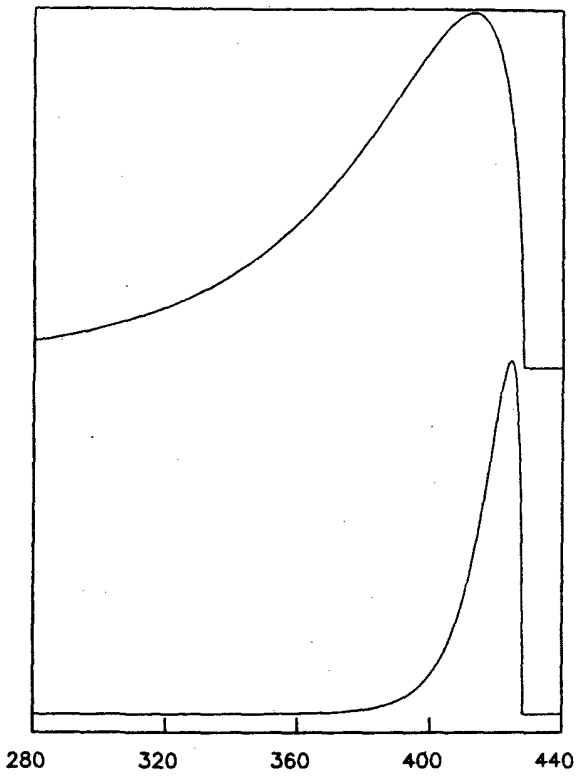

Figure 24. Selection of lineshapes for magnetic field induced resonance at a microwave frequency ν_c = 9.139 GHz. E = 0, E_0 = 200 MHz(lower) and 400 MHz (upper). (Figure courtesy of Mr. G.R.Sinclair).

Similar calculations for the electric field transitions with a sharp cut-off at B_u run into the problem that the final expression for S is proportional to $1/\Delta_c$.

In the theory given by Baker and Bleaney (98), and developed more fully by Abragam and Bleaney (1), an unnormalized chi-squared distribution is used. The lineshape expression is then transformed into the field domain in the form w(h)dh where h = $B_u - B$. This suffers from the error that the resulting expression has the wrong dimensions compared to $S(B, v_c)$.

In the biological context, Hagen and his associates have explored even electron states by means of what they call 'dual mode spectroscopy'. They had the option to detect the EPR signal with the microwave magnetic field either parallel to or perpendicular to the d.c. field and carried out such experiments on oxygen activated bovine heart cytochrome c-oxidase (102). In the parallel mode, features occur at effective g-factors of 10 and 4.5. The usual perpendicular mode EPR showed principal features corresponding to effective g-factors of 10, 5, 1.8 and 1.7. These can be explained using an $S = 2$ spin Hamiltonian with the fourth order cubic parameter, $|a| = 0.17 cm^{-1}$, second order fine structure parameters $D = 2.1\ cm^{-1}$ and $|E| = 0.026\ cm^{-1}$ and a g-factor ≈ 2.

Hagen, van Berkel-Arts, Kruse-Wolten, Dunham and Veeger (103) have found a novel high spin component in activated hydrogenase, an enzyme which catalyses the reversible oxidation of hydrogen to protons. In catalase from *Dsulfovibrio vulgaris* (Hidlenborough), which is believed to contain three [4Fe-4S] centers, a minor axial component is found with g-factors $\approx$ 2.06 and 2.01. In fully active reoxidized enzyme, a 'rhombic' signal is found whose principal g-factors of $\approx$ 2.11, 2.05 and 2.00 are similar to those found for other oxidized bi-directional hydrogenases. This is in addition to a novel $g = 5$ signal associated with an $S = 2$, $\Delta M = 2$ transition from the $|\pm 1>$ doublet.

Hagen, Dunham, Johnson and Fee (104) find a quarter field resonance in the EPR of thermus thermophilus ferredoxin, a protein which contains seven iron atoms. These presumably reside in a 4Fe and a 3Fe cluster with the reduced 3Fe cluster giving rise to the $\Delta M = 4$ transition similar to that for high spin Fe(III) EDTA. They consider all possible redox states of both clusters and conclude that the 3Fe center, when oxidized, has $g \approx 2$.

X. Spin Lattice Relaxation

The theory of paramagnetic relaxation required for proteins now requires consideration of the idea of a fractal or a fractional dimension (d) (105). Wagner et al. (106) present a geometrical model to interpret the anomalous T^{3+2m} dependence of the Raman spin lattice relaxation rate for Kramers ions in heme and iron sulfur proteins, where m is not necessarily an integer (see Figure 25). A modified Debye relationship where the vibrational density of states is dependent on ν^{m-1} is consistent with the values of m determined from measurements on cytochrome c-551 and putidaredoxin where the results show some dependence on choice of solvent.

The apparent physical significance of m is revealed, in part, by correlation to the protein fractal geometry. From independent data on 70 proteins it is known that $1 < d < 2$, while for the six proteins examined by Wagner et al. (106), $m = d$. It is interesting to note that $m = 5/3$ for a self-avoiding random walk. Scholes et al. (107) have measured the T_1 temperature dependence from pulsed EPR of Cu_A and heme a centers in cytochrome c oxidase. In the temperature range 1.5 – 20K, they report temperature dependences similar to those found by Wagner et al. (106), and conclude that $1/T_1$ varies approximately as $T^{6.5}$. This leads to a value of m $\approx$ 1.65. The authors conclude that either both Cu_A and heme a centers involve similar environments or that Cu_A is relaxed by a nearby heme group. Similar values of the spectral dimension m to those reported by Wagner et al. were found.

Orbach relaxation for high spin ferric heme proteins has been investigated by Brill et al (108). They report that for the aquo complex of sperm whale myoglobin at T < 4K, and for phonon energies $\approx$ 20 cm^{-1}, the density of vibrational states behaves like that of a 3-dimensional system. They conclude this from the pre-exponential factor which is proportional to D^3 as expected for a three dimensional system. In eqn. 3 the splitting parameter Δ is proportional to the D used by Brill et al. They point out that the precise structure of the phonon density of states for the Raman process, since it depends on shorter wavelength phonons, will be much more sensitive to the structural properties of proteins and will depend on d. Different values of

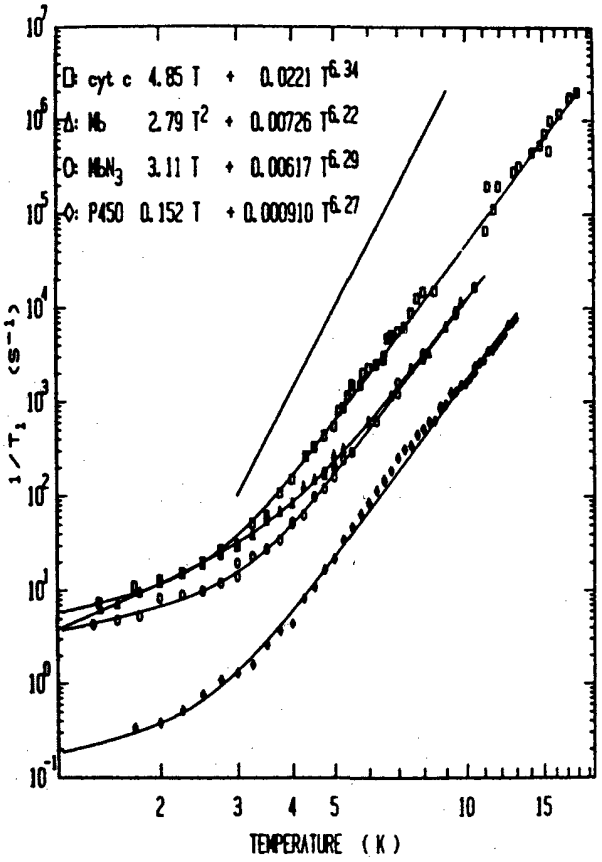

Figure 25. Relaxation rates (Allen, Colvin, Stinson, Flynn and Stapleton, *Biophys. J.*, **38**, 297 (1982) for four low spin hemoproteins (105) : ferricytochrome C (cyt c), myoglobin:OH (Mb), myoglobin azide (MbN_3), and cytochrome P450 from *Pseudomonas putida* (21). Each data set is separately fit to the sum of a direct process (varying with temperature as T or T^2) and a simple T^n power law. The best fitting values of n are indicated. Standard errors in n are typically 1%. The straight line represents a T^9 power law. For Mb and MbN_3 only every third datum is displayed between 5 and 11 K to improve clarity. An n value of 6.33 implies a spectral dimension of 5/3. All data corresponding to relaxation rates below 10^4 s^{-1} were measured at X-Band microwave frequencies ($\sim$ 9.5 GHz) on frozen protein solutions. The cytochrome C data above T = 10 K were taken on a single crystal using a microwave frequency of 24 GHz [C. Mailer and C. P. S. Taylor, *Biochim. Biophys. Acta* **322**, 195 (1973)] and have been reduced by a factor of 0.106. (Reproduced with permission of the author of ref. 105.)

d found for low spin and high spin heme proteins arise from the particular regions of phonon energy (or frequency) which produce the measured effect, rather than from differences in binding of metal ions in the macromolecule. Lewis et al. (109) describe EPR relaxation studies of the blue copper protein rusticyanin from the chemlithotropic bacterium *Thiobacillus ferredoxins.* Relaxation times measured by power saturation at low temperatures (6 – 80K) give evidence for a pronounced T^2 phonon bottleneck. In the range 17 – 50K, T^6 behavior is found where $m = d = 1.5$.

On a more conventional note, Makinen and his colleagues (22-24) have recently reported the determination of zero field splittings for a wide range of four, five and six coordinate cobalt (II) complexes by means of CW power saturation in a temperature region where the Orbach process dominates the relaxation (23). They find that a zero field splitting < 13 cm^{-1} corresponds to four- coordination, splittings $\approx 20 - 50$ $cm^{-1}$to five- coordination (trigonal bipyramidal and square pyramidal) and values ≥ 50 cm^{-1} to six-coordination. I quote from their abstract (Makinen et al. (23)) "On this basis, it is suggested that the splitting between the two lowest Kramers doublets of high spin Co^{2+} may provide a diagnostic signature of coordination geometry". Their motivation was to see if any light could be shed on the problem of Co-substituted enzymes, especially cobalt carboxypeptidase (CPA) alluded to earlier. In a later paper, Kuo and Makinen (24) consider the ligand environment of the active metal site of CPA in ester hydrolysis where they find the zero field splitting to be 8.3 cm^{-1} for the free enzyme, 51 cm^{-1} in enzyme-L-benzylsuccinate inhibitor complexes and 39 cm^{-1} in mixed anhydride reaction intermediates with o-(trans-p- chloro-m-cinnamoyl)-l-β-phenyllactate. They concluded that the free enzyme is four-coordinate, consistent with X-ray data and that the latter intermediate is five-coordinate. Such additional information may often help to resolve the questions that the *g*-factors alone do not.

XI. Conclusion

EPR, properly understood on the basis of quantum mechanical transition probability theory, leads to some new insights in relation to the usual field-swept experiments. It must be emphasised that the Quantum Mechanical transition probability theory

for the transition rate, expressed as Fermi's Golden Rule, has no analogue in the field-domain. The master eqn. 3, which includes the transition rate, describes both field and frequency sweep and requires no *a priori* assumption about detailed lineshapes in the field domain. Eqn. 3 has been used for $S = 5/2$ (2) in its more general form (25).

On the basis of eqn. 3, linewidth anisotropy, lineshape asymmetries and frequency dependent widths in hyperfine structure can now be consistently understood. This new level of understanding in EPR, while it seems obvious now, led the referee of our paper on asymmetric looping transitions in ruby (4) to say "this could and should have been done 25 years ago". So indeed! A number of trends in the practice of EPR can now be discerned which may point the way to new applications and insights in the future. While the spin Hamiltonian will remain of great importance as a short-hand way of representing the electronic ground states of transition ions, there is a definite trend towards interpreting the whole of a spectrum including lineshape detail. *There is a sense in which an EPR spectrum must be considered, in its own right, to be an important physical property of a paramagnetic system.* Not only has transition metal ion EPR matured in a great many respects in recent years, but the time is now ripe for new more routine applications to outstrip fundamental research. There are, it seems, opportunities in analytical chemistry, undergraduate teaching and perhaps even clinical medicine that have barely been explored.

While the main emphasis in transition ion EPR has been on solids, powders and frozen solutions, motional effects are now being recognized as of some importance. In fact some of the contributions to linewidths mentioned earlier could depend, in part, on dynamic effects. The continued growth of developments in the Jahn-Teller effect and the consequent recognition of vibronic coupling highlights the fact that it is naive to consider that a rigid model of a metal ion complex is at all a complete description of the situation. Furthermore, Hyde and others are showing that the methodology developed for spin labelling in the slow tumbling domain can be applied judiciously to slowly tumbling metal complexes.

There is also a growing understanding of the need for judicious multifrequency spectroscopy in EPR, especially greater use of lower microwave frequencies. In order for this to become a more significant part of EPR practice, improved understanding of the origin of the linewidths in the solid state and in solution are needed. Present levels of understanding of copper (II) EPR confirm that S-band is right for the former and X-band for the latter.

In connection with electronic structure, modelling is far from ideal. Crystal field theories and the simpler, algebraic forms of LCAO-MO theories still remain very popular. The more comprehensive numerical methods are still limited because of the gross approximations needed to keep calculations tractable when there are so many metal and ligand electrons to consider. In general, it can be said that symmetry based models, or what Gerloch calls global models, provide very little chemical or physical intuition. The one advantage of both SPM and AOM models is that any symmetry is as easy as any other to deal with. For example, the AOM model works better for lower symmetries. The effect of a single ligand can be considered independently and correlated with other meaningful chemical or bonding data. Clearly it would be advantageous to be able to carry out *routine* calculations of the unrestricted Hartree-Fock or even 'ab-initio' variety. That goal seems some way off.

A good place to end is with reference to a particularly significant paper which concerns the use of an EPR spectrum as a physical property of the system. Amongst the some 200 known genetic disorders in new-born children which manifest themselves in a general condition known as lactic acidosis, Moreadith et al. (110) describe a clinical study of one particular condition relating to deficient levels in the iron sulfur proteins of complex I of the mitochondrial respiratory chain. They found quite different EPR spectra for sub-mitochondrial particles obtained from a patient suffering from the condition compared with a normal patient used as the control. Their results indicate one way in which EPR could become the basis of methods of clinical diagnosis.

Shortly, we expect to begin a related study of cytochrome-c-oxidase deficiency in collaboration with a team at the Royal Children's Hospital in Melbourne. This has some significance for the point of view of this article, for it was the improved resolution found by Hyde and Froncisz (6) in 1978 in the S-band EPR of that enzyme which opened up many of the issues raised here.

It was necessary to leave out any reference to interacting systems and pair interactions but some

relevant recent articles are included (111-118). Attention is drawn to the CODATA Bulletin No. 63 (Pergamon Press), edited by Cohen and Taylor(NBS), containing the most recent list of fundamental constants.

Acknowledgments

Much of what has been included in this article stems from many discussions between the author and Professor James S. Hyde during a sabbatical at the National Biomedical ESR Center during 1979. Other acknowledgments are due to my colleagues, G.J. Troup, D.R. Hutton and T.D. Smith and to the following members of my group, G.R. Sinclair, Feng Yi, D.M. Wang, and N.R. McLaren. Discussions or correspondence with the following is also acknowledged: A.G. Wedd, G.R.Hanson, G.L. Wilson, B.L.Vallee, B. Holmquist, A.S. Brill, W.R. Hagen, C.P. Keijzers and P.G. Debrunner.

References

[1]A. Abragam and B. Bleaney, "Electron Paramagnetic Resonance of Transition Ions", Clarendon Press, Oxford (1970).

[2]R. E. Coffman, *J. Phys. Chem.* **79**, 1129 (1975).

[3]R. Aasa and T. Vanngard, *J. Magn. Res.* **19**, 308 (1975).

[4]J. R. Pilbrow, G. R. Sinclair, D. R. Hutton and G. J. Troup, *J. Magn. Res.* **52**, 386 (1983).

[5]J. R. Pilbrow, *J. Magn. Res.* **58**, 186 (1984).

[6]J. R. Pilbrow, Proc. 2nd Asia Pacific Physics Conference, Bangalore, India, January 1986 (Ed. S. Chandrasekhar), World Scientific, Singapore (1986), Vol. 2, 914.

[7]W. Froncisz, C. P. Scholes, J. S. Hyde, Y. H. Wei, T. E. King, R. W. Shaw and H. Beinert, *J. Biol. Chem.* **254**, 7482 (1979).

[8]W. Froncisz and J. S. Hyde, *J. Chem. Phys.* **73**, 3123 (1980).

[9](a) I. B. Bersuker, "The Jahn-Teller Effect and Vibronic Interactions in Modern Chemistry", Plenum, New York (1984).

[9](b) Yu. E. Perlin and M. Wagner (Eds.), "The Dynamical Jahn-Teller Effect in Localized Systems", Elsevier (1984).

[10]M. T. Hutchings, *Solid State Physics* (F. Seitz and D. Turnbull, Eds.) **16**, 227 (1964).

[11]D. J. Newman and W. Urban, *Adv. Phys.* **24**, 793 (1975).

[12]M. Gerloch, "Magnetism and Ligand Field Analysis", Cambridge University Press, 1983.

[13]M. H. L. Pryce, *Proc. Phys. Soc.* **A63**, 25 (1950).

[14]A. Abragam and M. H. L. Pryce, *Proc. Roy. Soc. A.* **205**, 135 (1951).

[15]C. Rudowicz, *Magn. Res. Revs.* **13**, 1 (1987).

[16]G. E. Pake and T. L. Estle, "The Physical Principles of Electron Paramagnetic Resonance", W. A. Benjamin, New York, 1973.

[17]J. F. Boas, J. R. Pilbrow and T. D. Smith, *In* "Biological Magnetic Resonance" (L. J. Berliner and J. Reuben, Eds.) **1**, 227 (1978).

[18]A. H. Maki and B. R. McGarvey, *J. Chem. Phys.* **29**, 31 (1958)

[19]C. P. Keijzers and E. deBoer, *Molec. Phys.* **29**, 1007 (1975).

[20]R. Orbach and H. J. Stapleton, *In* "Electron Paramagnetic Resonance" (S. Geschwind, Ed.) Plenum, New York, 1972, p. 121.

[21]R. C. Herrick and H. J. Stapleton, *J. Chem. Phys.* **65**, 4778 (1976).

[22]M. B. Yim, L. C. Kuo and M. W. Makinen, *J. Magn. Res.* **46**, 247 (1982).

[23]M. W. Makinen, L. C. Kuo, M. B. Yim, G. B. Wells, J. M. Fukuyama and J. E. Kim, *J. Am. Chem. Soc.* **107**, 5245 (1985)

[24]L. C. Kuo and M. W. Makinen, *J. Am. Chem. Soc.* **107**, 5255 (1985).

[25]C. P. Slichter, "Principles of Magnetic Resonance", Harper and Row, New York, 1963, pp. 40-44 and Appendix E.

[26]G. Dougherty, J. R. Pilbrow, A. Skorobogaty and T. D. Smith, *J. Chem. Soc. Faraday* **2**, **81**, 1739 (1985).

[27]E. O. Schulz-duBois, *Bell Syst. Tech. J.* **38**, 271 (1959).

[28]G. R. Sinclair, M. Sc. thesis, Monash University (1983).

[29]*J.R.Pilbrow, J.Magn.Res.***31**, 479(1978).

[30]P. L. Scott, H. J. Stapleton and C. Wainstein, *Phys. Rev.* **A137**, 71 (1965).

[31]W. R. Hagen, *J. Magn. Res.* **44**, 447 (1981).

[32]D. O. Hearshen, W. R. Hagen, H. J. Grande, H. J. Crespi, I. C. Gunsalus and W. R. Dunham, *J. Magn. Res.* **69**, 440 (1986).

[33]W. R. Hagen, D. O. Hearshen, R. H. Sands and W. R. Dunham, *J. Magn. Res.* **61**, 220 (1985).

[34]W. R. Hagen, D. O. Hearshen, L. J. Harding and W. R. Dunham, *J.Magn.Res.***61**,233(1985).

[35]W. N. Hardy and L. A. Whitehead, *Rev. Sci. Instr.* **52**, 213 (1981).

[36]J. S. Hyde and W. Froncisz, Proc. Nat. Electronics Conf. USA, **XXXV**, 602 (1982).

[37]W. Froncisz and J. S. Hyde, *J. Magn. Res.* **47**, 515 (1982).

[38]J. R. Anderson, R. A. Venters, M. K. Bowman, A. E. True and B. M. Hoffman, *J. Magn. Res.* **65**, 165 (1985).

[39]J. S. Hyde and W. Froncisz, *Ann. Rev. Biophys. Bioeng.* **11**, 391 (1982).

[40]G. R. Hanson, Ph. D. thesis, Latrobe University (1984).

[41]G. R. Hanson, G. L. Wilson, T. D. Bailey, J. R. Pilbrow and A. G. Wedd, *J. Am. Chem. Soc.* **109**, 2609 (1987).

[42]F. Farchione, G. R. Hanson, C. D. Rodrigues, T. D. Bailey, R. N. Bagchi, A. M. Bond, J. R. Pilbrow and A. G. Wedd, *J. Am. Chem. Soc.* **108**, 831 (1986).

[43]G. J. Troup, D. R. Hutton and J. R. Pilbrow, *J. Gemmol.* **XIX**, 431 (1985).

[44]J. Baldas, J. F. Boas, J. Bonnyman, J. R. Pilbrow and G. R. Williams, *J. Am. Chem. Soc.* **107**, 1886 (1985).

[45]J. F. Boas and J. R. Pilbrow, *Phys. Rev. B* **32**, 8258 (1985).

[46]R. Sealy, J. S. Hyde and W. E. Antholine, *In* "Modern Physical Methods in Biochemistry", Ed. A. Neuberger and L. L. M. Van Deenen, Elsevier, New York, 1985, p. 69.

[47]K. S. Rothenberger, M. J. Nilges, T. E. Altman and R. L. Belford, *Chem. Phys. Lett.* **124**, 295 (1986).

[48]G. Rakhit, W. E. Antholine, W. Froncisz, J. S. Hyde, J. R. Pilbrow, G. R. Sinclair and B. Sarkar, *J. Inorg. Biochem.* **25**, 217 (1985).

[49]R. Basosi, G. Valencia, E. Gaggelli, W. Froncisz, M. Pasenkeiwicz-Gierula, W. E. Antholine and J. S. Hyde, *Inorg. Chem.* **25**, 3006 (1986).

[50]M. Pasenkiewicz-Gierula, W. Froncisz, R. Basosi, W. E. Antholine and J. S. Hyde, *Inorg. Chem.* **26**, 801 (1987).

[51]J. S. Hyde, W. E. Antholine and R. Basosi, **In** "Biological and Inorganic Copper Chemistry", (K. D. Karlin and J. Zubieta, Eds.) Adenine Press, 1985, p. 239.

[52](a) H. Hosono, H. Kawazoe and T. Kanazawa, *J. Non-Cryst. Solids* **33**, 103 (1979); (b) H. Kawazoe, H. Hosono, H. Kokumai, J. Nishi and T. Kanazawa, *J. Non-Cryst. Solids* **40**, 291 (1980).

[53]A. Papoulis, "Probability, Random Variables and Stochastic Processes", McGraw Hill, New York, 1965.

[54]A. S. Brill and D. A. Hampton, *Biophys. J.* **25**, 313 (1979).

[55]J. H. Van Vleck, *Phys. Rev.* **74**, 1168 (1948).

[56]G. R. Sinclair and J. R. Pilbrow, unpublished (1987).

[57]W. H. Robinson and S. D. Devine, *Adv. Mag. Res.* **10**, 53 (1982).

[58]C. P. Keijzers, private communication (1985).

[59]E. J. Reijerse, N. A. J. M. van Aerle, C. P. Keijzers, R. Bottcher, R. Kirmse and J. Stach, *J. Magn. Res.* **67**, 114 (1986).

[60]J. R. Pilbrow and J. -M. Spaeth, *Phys. Stat. Sol.* **20**, 225 (1967).

[61]D. A. Hampton and A. S. Brill, *Biophys. J.* **25**, 301 (1979).

[62]G. A. Helke, D. J. E. Ingram and E. F. Slade, *Proc. Roy. Soc. B.* **169**, 275 (1968).

[63]F. Fiamingo, R. Thorkildsen and A. S. Brill, *Biophys. J.* **25**, 301 (1979).

[64]A. S. Brill, F. Fiamingo and D. A. Hampton, *Biophys. J.* **28**, 137 (1986).

[65]Feng Yi, private communication (1987).

[66]G. E. Peterson, C. R. Kurkjian and A. Carnevale, *J. Phys. Chem. Glasses* **15**, 52 (1974).

[67]A. Carnevale, G. E. Peterson and C. R. Kurkjian, *J. Non-Cryst. Solids* **22**, 269 (1976).

[68]G. Guigliarello and S. Cannistraro, *Chem. Phys.* **98**, 115 (1985).

[69]S. Cannistraro and G. Guigliarello, *Molec. Phys.* **58**, 173 (1986).

[70]C. K. Wang, G. Guigliarello and S. Cannistraro, *Il Nuovo Cimento* **8**, 76 (1986).

[71]J. S. Hyde and J. R. Pilbrow, *J. Magn. Res.* **41**, 447 (1980).

[72]M. Pasenkiewicz-Gierula and J. S. Hyde, *J. Magn. Res.* submitted (1987).

[73]R. L. Belford and J. R. Pilbrow, *J. Magn. Res.* **11**, 381 (1973).

[74]Powder simulation program QPOW supplied by Professor R. L. Belford. Program diagonalizes energy matrix at center of hyperfine spectrum for each orientation.

[75]Program QPOWFS is version of QPOW modified by G. R. Sinclair using eqn. 3 and energy dif-

ferences between eigenvalues.

[76]J. E. Lennard-Jones, *Proc. Roy. Soc. A* **129**, 1854 (1958).

[77]D. B. Fulton, R. Skinner and J. A. Weil, *J. Magn. Res.* **69**, 41 (1986).

[78]R. Skinner and J. A. Weil, *J. Magn. Res.* **21**, 271 (1976).

[79]R. Skinner and J. A. Weil, *J. Magn. Res.* **29**, 223 (1978).

[80]G. Van Veen, *J. Magn. Res.* **30**, 91 (1978).

[81]R. Stevenson, *J. Magn. Res.* **57**, 24 (1984).

[82]G. A. Korteweg, *J. Magn. Res.* **42**, 181 (1981).

[83]P. W. Kennedy, Ph. D. thesis, Monash University (1978).

[84]M. I. Scullane, L. K. White and N. D. Chasteen, *J. Magn. Res.* **47**, 383 (1982).

[85]G. R. Sinclair, J. R. Pilbrow, D. R. Hutton and G. J. Troup, *J. Magn. Res.* **57**, 228 (1984).

[86]A. Schweiger, *J. Magn. Res.* **51**, 286 (1983).

[87]A. Schweiger, Struct. Bond., **57**, 1 (1981).

[88]J.-M. Spaeth and J. R. Niklas, (a) *Phys. Stat. Sol. (B)* **101**, 221 (1980), (b) *In* "Recent Developments in Condensed Matter Physics", Vol. 1, J. T. Devreese, Ed., Plenum, New York 1981, p. 393.

[89]D. M. Wang, D. R. Hutton and J. R. Pilbrow, *J. Phys. Chem.* **19**, 789 (1986).

[90]D. M. Wang, D. R. Hutton, G. J. Troup and H. P. Jenssen, *Phys. Stat. Sol. (A)* **98**, 98 (1986).

[91]D. M. Wang and J. R. Pilbrow, *J. Magn. Res.* in press (1988).

[92]W. Waller and M. T. Rogers, *J. Magn. Res.* **9**, 92 (1973).

[93]L. Banci, A. Bencini, C. Benelli, D. Gatteschi and C. Zanchini, *Struct. Bond.* **52**, 37 (1982).

[94] (a)K. F. Geohagen, A. Galdes, G. Hanson, B. Holmquist, D. S. Auld and B. L. Vallee, *Biochem.* **25**, 4669 (1986); (b)R. A. Martinelli, G. R. Hanson, J. S. Thompson, B. Holmquist, J. R. Pilbrow, D. S. Auld and B. L. Vallee, *Biochem.*, submitted (1988).

[95]W. R. Hagen, R. R. Eady, W. R. Dunham and H. Haaker, *FEBS* **189**, 250 (1985).

[96]D. J. Lowe and B. E. Smith, *Biochem. Soc. Trans.* **13**, 579 (1985).

[97]G. R. Sinclair and J. R. Pilbrow, *J. Magn. Res.* submitted (1987).

[98]J. M. Baker and B. Bleaney, *Proc. Roy. Soc. A* **245**, 156 (1958).

[99]F. I. B. Williams, *Proc. Phys. Soc. A* **91**, 111 (1967).

[100]R. S. Anderson, C. A. Bates and P. C. Jassaud, *J. Phys. Chem.* **5**, 3397 (1972).

[101]W. S. Moore, C. A. Bates and T. M. Al Shabarti, *J. Phys. Chem.* **6**, 1209 (1973).

[102]W. R. Hagen, W. R. Dunham, R. H. Sands, R. W. Shaw and H. Beinert, *Biochim. Biophys. Acta* **765**, 399 (1984).

[103]W. R. Hagen, A. vanBerkel-Arts, K. M. Kruse-Wotter, W. R. Dunham and C. Veeger, *FEBS* **201**, 158 (1986).

[104]W. R. Hagen, W. R. Dunham, M. K. Johnson and J. A. Fee, *Biochim. Biophys. Acta* **828**, 369 (1985).

[105]H. J. Stapleton, Lecture, Frohlich Symposium, Sanibel Island, Florida (1985).

[106]G. S. Wagner, J. T. Colvin, J. P. Allen and H. J. Stapleton, *J. Am. Chem. Soc.* **107**, 5589 (1985).

[107]C. P. Scholes, R. Janakiram, H. Taylor and T. E. King, *Biophys. J.* **45**, 1027 (1984).

[108]A. S. Brill, F. Fiamingo, D. A. Hampton, P. D. Levin and R. Thorkildsen, *Phys. Rev. Lett.* **54**, 1864 (1985).

[109]C. A. Lewis, W. J. Ingledew and A. G. Lappin, *Biochem. Soc. Trans.* **13**, 634 (1985).

[110]R. W. Moredith, M. L. Batshaw, T. Ohnishi, D. Kerr, B. Knox, D. Jackson, R. Hruban, J. Olson, B. Reynafarjea and A. Lehninger, *J. Clin. Invest.* **74**, 685 (1984).

[111]C. P. Keijzers, "Specialist Periodical Reports - Electron Spin Resonance" (M. C. R.Symons, Ed.) **10B**, 1987, p. 1.

[112]S. S. Eaton and G. R. Eaton, "Biol. Magn. Res." (L. J. Berliner and J. Reuben, Eds.) Plenum, New York, 1987, in press.

[113]S. S. Eaton and G. R. Eaton, *Coordin. Chem. Rev.*, in press.

[114]D. Snaathorst and C. P. Keijzers, *Molec. Phys.* **51**, 509 (1984)

[115]M. A. Hefni, N. M. McConnell, F. J. Reitmeijer, M. C. N. Gribnau and C. P. Keijzers, *Molec. Phys.* **57**, 1283 (1986).

[116]B. Guigliarelli, J. P. Gayda, P. Bertrand and C. More, *Biochim. Biophys. Acta* **871**, 149 (1986).

[117]B. Guigliarelli, P. Bertrand and J. P. Gayda, *J. Chem. Phys.* **85**, 1689 (1986).

[118]B. Guigliarelli, C. More, P. Bertrand and J. P. Gayda, *J. Chem. Phys.* **85**, 2774 (1986).